A novel subset of hepatocytes is simultaneously gluconeogenic and *de novo* lipogenic in the fed state and is naturally insulin resistant

Junichi Okada[1], Austin Landgraf[2], Maxwell Horton[2,3], Yunping Qiu[1,4], Alus M. Xiaoli[1,5], Roberto Ribas[6], Li Liu[1], Sofia V. Krylova[2], Hernando J. Olivos[7], Victor L. Schuster[8], Fajun Yang[1,5], Takeshi Saito[9], Ramon C. Sun[6,10,11], Meredith Hawkins[1], Gary J Schwartz[1,12,13], Carolina Eliscovich[5,14], Kosaku Shinoda[1,2], Irwin J. Kurland[1,4] and Jeffrey E. Pessin[1,2]

[1]Departments of Medicine (Division of Endocrinology), [2]Molecular Pharmacology, [3]Biochemistry, [5]Developmental and Molecular Biology, [8]Medicine (Division of Nephrology), [12]Neuroscience, [13]Psychiatry and Behavioral Sciences and [14]Medicine (Hepatology). [4]Stable Isotope and Metabolomics Core Facility, New York Regional Diabetes Research Center. Fleischer Institute for Diabetes and Metabolism, The Albert Einstein College of Medicine, Bronx, NY 10461

[6]Department of Biochemistry and Molecular Biology, College of Medicine, University of Florida, Gainesville, FL 32610

[7]Waters Corporation, Milford, MA 01757

[9]Department of Medicine, Division of Gastrointestinal and Liver Diseases, Immunology & Immune Therapeutics, and Pathology, Keck School of Medicine, University of Southern California, Los Angeles, CA 90033

[10]Center for Advanced Spatial Biomolecule Research, University of Florida, Gainesville, FL 32610

[11]Evelyn F. and William L. McKnight Brain Institute, University of Florida, Gainesville, FL 32610

Please address correspondences to:

Junichi Okada
Department of Medicine (Division of Endocrinology)
The Albert Einstein College of Medicine
369 Price Center, 1301 Morris Park Avenue
Bronx, NY 10461
Email: junichi.okada@einsteinmed.edu

ABSTRACT

It is generally accepted that hepatic gluconeogenesis, the synthesis of glucose from non-carbohydrate substrates is active in the fasted state and inactive in the fed state. In contrast, *de novo* lipogenesis is active in the fed state and is inactive in the fasted state. Here, we used targeted single cell RNA-seq, HCR RNA-FISH, and PrimeFlow in normal physiological mouse liver, and identified a subpopulation of periportal hepatocytes that simultaneously co-express both gluconeogenic and lipogenic genes in the fed state. Euglycemic-hyperinsulinemic clamps further demonstrated that this novel hepatocyte subpopulation is naturally insulin resistant. Spatial metabolic imaging coupled with stable isotope tracing analyses revealed individual hepatocytes that simultaneously undergo both gluconeogenesis and *de novo* lipogenesis. These dual-positive hepatocytes were also present in human hepatocytes from humanized mouse livers. Moreover, the number of dual-positive hepatocytes increased in high-fat diet-fed mice, suggesting a paradigm shift in our understanding of how the liver becomes insulin resistant.

INTRODUCTION

The mammalian liver is composed of parenchymal (hepatocytes) and non-parenchymal (endothelial, Kupffer, cholangiocytes, stellate) cells organized into repetitive hexagonal arrays termed lobules[1,2]. Within each lobule the hepatocytes are distributed from the portal triad (portal vein, hepatic artery, bile duct) at the six vertices and the central vein located at the centroid of the hexagon. The hepatocytes aligned within a lobule display functionally distinct metabolic properties and are generally

98 divided into three zones: the periportal hepatocytes (zone 1), midlobular hepatocytes
99 (zone 2) and the pericentral hepatocytes (zone 3), with emerging single-cell studies
100 indicating that hepatic zonation exists along a more continuous and finely partitioned
101 spectrum[3,4]. The pericentral hepatocytes display higher rates of glycolysis, bile acid and
102 glutamine biosynthesis[1,2]. The periportal hepatocytes are primarily responsible for beta-
103 oxidation and urea oxidation and in particular, gluconeogenesis[1,2]. However,
104 gluconeogenesis is a dynamic process that is regulated by numerous hormonal, neural
105 and metabolic inputs. During early states of fasting *in vivo*, we found that periportal
106 hepatocytes are initially responsible for gluconeogenesis, but as fasting duration
107 increased, the mid-zone and then pericentral hepatocytes underwent increased
108 gluconeogenic gene expression, protein levels and ultimately gluconeogenic activity that
109 approached that of the periportal hepatocytes[5]. In contrast, lipogenic gene expression
110 that is high in the fed state is rapidly downregulated to essentially undetectable levels
111 during the initial time frame of fasting induction. These data demonstrate the remarkable
112 plasticity of hepatocyte gluconeogenic gene expression and gluconeogenic activity
113 across the liver lobule depending upon organismal nutrient state.
114 While it is generally accepted that *de novo* lipogenesis is activated in the fed state
115 whereas gluconeogenesis and hepatic glucose output are activated in the fasted state,
116 several studies observed a measurable rate of gluconeogenesis and hepatic glucose
117 production in the fed state, despite the availability of dietary glucose[6,7]. Although not
118 thoroughly investigated, the molecular and cellular bases for the basal rate of hepatic
119 gluconeogenesis and hepatic glucose output was generally thought to represent
120 glucose production for the indirect pathway of glycogen synthesis[8-11].

121 In this study, we used a variety of single cell technologies to confirm the presence of
122 basal liver gluconeogenic activity transcriptionally and functionally in the fed state that
123 results in hepatic glucose release. Importantly, our data revealed that this basal
124 gluconeogenesis results from a subset of unique hepatocytes that simultaneously
125 display expression of both *de novo* lipogenic and gluconeogenic genes exclusively
126 localized to the periportal region. Spatial metabolomic imaging further confirmed that
127 this subset of periportal hepatocytes is capable of simultaneously undergoing both
128 gluconeogenesis and *de novo* lipogenesis, and have high rates of ATP turnover,
129 consistent with the energetic need to sustain these dual processes. Furthermore,
130 euglycemic-hyperinsulinemic clamps and PrimeFlow analyses suggested that these
131 hepatocytes are resistant to insulin suppression of gluconeogenic gene expression,
132 demonstrating natural insulin resistance under normal physiological conditions.
133 Moreover, the number of these naturally insulin-resistant hepatocytes is increased by
134 high-fat diet feeding.
135

136 **RESULTS**

137 **Gluconeogenic genes are transcribed in hepatocytes in the fed state**

138 To investigate the regulation of liver gene expression in the normal physiological
139 transitions between fed and fasted states, we used a previously established protocol in
140 which mice rapidly consume food and fill their stomachs to create a relatively uniform
141 fed state, and following food removal, facilitate a uniform transition into the fasted
142 state[5,12]. We first confirmed our previous findings that lipogenic gene *Fasn* mRNA is
143 highly expressed in the fed state of total primary isolated hepatocytes and nearly

144 completely suppressed in the fasted state (Fig. 1A). In contrast to lipogenic gene
145 mRNA, the gluconeogenic gene *Pck1,* was highly expressed in the fasted state, yet
146 surprisingly there was a low but readily detectable mRNA in the fed state as well (Fig.
147 1B). There were no significant effects of fasting/feeding on the expression of
148 constitutively expressed gene albumin (*Alb*) mRNA (Fig. 1C). To determine if the
149 observed feeding state changes in mRNA levels were due to a transcriptional process,
150 we examined the transcriptional activation of lipogenic and gluconeogenic genes by
151 performing DNA-dependent RNA polymerase II (RNAPII) ChIP-seq to assess RNAPII
152 gene occupancy in total primary isolated hepatocytes. As expected, RNAPII occupancy
153 was relatively high across the gene body of *Fasn* in the fed state with very low binding
154 in the fasted state (Fig. 1D). RNAPII occupancy on other lipogenic genes *Acly* and
155 *Elovl6*, displayed a similar pattern (Fig. S1A and S1B). Both *Fasn* and *Acly* displayed a
156 peak of RNAPII at the transcription start site indicative of proximal promoter pausing[13].
157 In contrast, the gluconeogenic genes *Pck1* and *G6pc* showed the opposite trend with
158 higher RNAPII occupancy in the fasted state. Although both *Pck1* (Fig. 1E) and *G6pc*
159 (Fig. S1C) displayed strong gene occupancy by RNAPII in their active (fasted) state, we
160 also observed RNAPII gene occupancy in the inactive fed state. In addition, there was
161 no evidence of proximal promoter pausing for the gluconeogenic genes. In contrast,
162 there were no changes in RNAPII occupancy for *Alb* (a constitutive hepatocyte gene,
163 Fig. 1F). As a control, the *Ins1* gene, which is not expressed in hepatocytes, showed
164 virtually no RNAPII occupancy in either the fed or fasted state (Fig. 1G).
165 The apparent transcription of gluconeogenic genes in the fed state could occur in all
166 hepatocytes or be restricted to a subset of hepatocytes. To explore these possibilities,

167 we isolated pericentral and periportal hepatocytes from fed and 16 h fasted mice using
168 a digitonin ablation method that we modified for application in mice[5,14,15]. The isolated
169 pericentral (PC) and periportal (PP) hepatocytes were then subjected to RNAPII ChIP-
170 seq analyses. To confirm the relative purity of separation we examined the mRNA
171 expression levels of *Cyp2e1*, an established PC hepatocyte marker, and *Cyp2f2*, an
172 established PP marker[3,5,16]. As shown in Figure S2A there was a ~ 6 to 9-fold
173 enrichment of *Cyp2e1* in the PC hepatocytes and an ~ 4 to 6-fold enrichment of *Cyp2f2*
174 in the PP hepatocytes (Fig. S2B).
175 RNAPII ChIP-seq demonstrated that *Fasn* gene was transcriptionally active in both
176 the PC and PP hepatocytes in the fed state, although somewhat greater in the PP
177 hepatocytes (Fig. S2C). The *Fasn* gene occupancy of RNAPII in both PC and PP
178 hepatocytes is consistent with the mRNA expression of lipogenic genes levels across
179 the liver lobule[5]. In any case, in the fasted state there was essentially no RNAPII
180 occupancy of *Fasn* gene in either PC or PP hepatocytes with the proximal promoter
181 pausing peak readily observable in both zones. As expected in the fasted state, RNAPII
182 occupancy of the *Pck1* gene was high in both the PC and PP hepatocytes (Fig. S2D),
183 consistent with *Pck1* mRNA expression that is also expressed in both PC and PP
184 hepatocytes following long-term fasting[5]. However, in contrast to *Fasn* gene, in the fed
185 "off-state" *Pck1* gene still displayed substantial RNAPII occupancy in the PP
186 hepatocytes but nearly background levels in the PC hepatocytes (Fig. S2D). As
187 controls, RNAPII occupancy of *Alb* was neither zonated nor responsive to
188 fasting/feeding (Fig. S2E) and the RNAPII tracks for *Ins1* was essentially background

189 (Fig. S2F). These data indicate that the basal (fed state) transcription and expression of
190 gluconeogenic genes occur predominantly in PP hepatocytes.
191
192 **Lipogenic and gluconeogenic genes are co-expressed in a subset of periportal**
193 **hepatocytes**
194 We next addressed whether all PP hepatocytes or a subset of PP hepatocytes were
195 responsible for the basal expression of gluconeogenic genes in the fed state. To
196 address this, we first utilized quantitative targeted single cell RNA-seq (targeted scRNA-
197 seq) using the 10x genomic platform for a selective subset of metabolic genes[5]. Cell
198 ranger and Loupe Browser were used for analyses for the quantitative targeted scRNA-
199 seq to establish UMAP cluster maps of the hepatocytes in the fully fed and fasted states
200 (Fig. 2A). To identify the position of the PC and PP hepatocytes (Fig. 2B) we took
201 advantage of previous studies that have characterized the localization of specific
202 zonation markers[3,5,16]. As examples, the PC markers *Cyp2e1* and *Gulo* (Fig. 2C) were
203 highly colocalized to one region whereas the PP markers *Cyp2f2* and *Hsd17b13* (Fig.
204 2D) were highly colocalized to another distinct region. As these genes are typically
205 expressed as a gradient across the lobule, (with the notable exception of *Glul* that is
206 highly restricted to hepatocytes in one to two layers around the central vein), the other
207 lower expressing cells likely represent the mid-zone hepatocytes[1,5]. As expected, in the
208 fully fed state, the *de novo* lipogenic gene *Fasn* was found in both the PC and PP
209 hepatocytes but following fasting was essentially absent from all the hepatocytes (Fig.
210 2E). On the other hand, the gluconeogenic gene *Pck1* was expressed in both the PC
211 and PP hepatocyte clusters in the fasted state, but also showed expression in a subset

212 of PP, but not PC, hepatocytes in the fed state (Fig. 2F). Alignment of the UMAPs for
213 the hepatocytes that co-express both *Fasn* and *Pck1* mRNA in the fed state indicated
214 they account for 7% of the periportal hepatocytes (Fig. 2G). In addition, comparison of
215 other core *de novo* lipogenic genes (*Acly*, *Acaca*, and *Elvol6*) with the gluconeogenic
216 gene *G6pc* also demonstrated that approximately 19% of PP hepatocytes
217 simultaneously co-expressed these mRNAs (Fig. S3A-E).
218

219 **_Fasn_ and _Pck1_ are actively co-transcribed in a subset of periportal hepatocytes**

220 To confirm the scRNA-seq identification of a periportal hepatocyte subset that
221 simultaneously expresses both gluconeogenic and *de novo* lipogenic genes, we utilized
222 Hybridization Chain Reaction RNA Fluorescence *in Situ* Hybridization (HCR RNA-FISH)
223 to simultaneously visualize the transcription sites (TS) of the *Fasn* and *Pck1* genes.
224 Simultaneous glutamine synthetase RNA-FISH was used to identify the PC region
225 (Figure 3, *Glul* not shown)[1,5]. In the fed state *Fasn* TS were readily observed throughout
226 the lobule but fewer *Pck1* TS were detected in a subset of the PP but not PC
227 hepatocytes (Fig. 3A, Fig. S4A and S4B). Magnified images clearly demonstrated the
228 presence of both *Fasn* and *Pck1* TS simultaneously in the same nucleus in a subset of
229 the PP hepatocytes (Fig. 3B). Quantification indicated that 24 % of the periportal
230 hepatocytes and 1 % of the pericentral hepatocytes displayed TS for both *Fasn* and
231 *Pck1* in the fed state (Fig. 3C). On the other hand, in the fasted state, *Pck1* TS was
232 readily detected throughout the lobule but with essentially no *Fasn* TS (Fig. 3D, Fig.
233 S4C and S4D). Magnified images of TS in the fasted state are shown in Fig. 3E.
234 Quantification indicated that hepatocytes that were dual-positive of TS were not

235 detected (Fig. 3F). These data directly demonstrate that the subset of PP hepatocytes
236 actively transcribed both lipogenic (*Fasn*) and gluconeogenic (*Pck1*) genes at the same
237 time.
238
239 **Periportal hepatocytes have basal pyruvate-to-glucose flux in the fed state**
240 Gene transcription and mRNA expression does not necessarily indicate functional
241 activity; we therefore directly determined the relative *de novo* lipogenesis and
242 gluconeogenesis activities by quantifying the fractional incorporation of $^{2}H_2O$ into
243 palmitate and [2,3-$^{13}C_2$] pyruvate into glucose (Fig. 4). As expected, the fractional
244 amount of ^{2}H-palmitate in total hepatocytes from the fed state was substantially higher
245 (16-fold) compared to hepatocytes from the fasted state (Fig. 4A). The decomposition of
246 this overall palmitate enrichment is shown as the increased fed vs. fasted isotopologue
247 enrichment distribution (Fig. 4B). This large increase appears to result from the very low
248 fractional synthesis in the fasted state. Conversely, the average ^{13}C incorporated per
249 molecule of glucose synthesized was higher (2.4-fold) in the hepatocytes from the
250 fasted state compared to the fed state (Fig. 4C). The decomposition of the isotopologue
251 distribution of glucose is shown in Figure 4D with the majority of glucose isotopologues
252 synthesized as either M2- or M4-glucose. To address the potential zonation of both
253 glucose and palmitate synthesis, we next examined the relative synthesis rates in
254 isolated PC and PP hepatocytes.
255 Consistent with *Fasn* gene expression, *de novo* lipogenesis activity is relatively high
256 in the fully fed state (Fig. 4E) with very low activity in the fasted state and exhibits
257 similar levels between PC and PP hepatocytes. The fold stimulation from the fasted “off”

258 state and the active fully fed “on” state is approximately 30-fold in PC and 55-fold in PP
259 hepatocytes. The isotopologue distribution of palmitate is shown in Figure 4F. In
260 contrast, in the fed state there is a low level of gluconeogenesis from isolated PC
261 hepatocytes, but it is several-fold higher in the PP hepatocytes (Fig. 4G). In the fasted
262 state, both PC and PP hepatocytes display a higher rate of gluconeogenesis.
263 Importantly, the PC hepatocytes increase their gluconeogenic activity ~10-fold, whereas
264 the PP hepatocytes only increase their gluconeogenic activity ~4-fold due to the higher
265 basal activity (Fig. 4G). The isotopologue distribution of glucose is shown in Figure 4H,
266 which again shows mainly the formation of M2- and M4-glucose. These data
267 demonstrate that in the fed state, PP hepatocytes display a significant degree of
268 gluconeogenic activity, consistent with the PP expression of gluconeogenic genes in the
269 fed state. On the other hand, PC hepatocytes exhibit a metabolic plasticity which
270 enables them to become equally gluconeogenic in the fed to fasted transition.
271

272 **Dual-positive hepatocytes are insulin resistant in suppression of *Pck1***

273 Since the fed state is a normal physiologically anabolic state primarily driven by
274 insulin, the expression of *Pck1* in the fed state suggests that this subset of PP
275 hepatocytes was less responsive to insulin (i.e., insulin resistant), at least to insulin
276 suppression of *Pck1* gene expression and gluconeogenic activity. To address this, we
277 established a quantitative assay to isolate these dual expression (*Fasn* and *Pck1*)
278 hepatocytes using PrimeFlow that is a combination of *in situ* hybridization coupled with
279 flow cytometry[17]. As shown in Figure S5A hepatocytes are relatively large cells with a
280 broad forward (FSC-A) and side scatter (SSC-A) parameters. Primary hepatocytes also

281 display background fluorescence in the APC-Cy7 and mCherry channels, which were
282 used for the *Pck1* and *Fasn* fluorescent mRNA probes (Fig. S5B). Nevertheless, in the
283 fed state there is a substantial increase in the *Fasn* signal, resulting in 75 % of
284 hepatocytes positive for *Fasn* (Fig. S5C). Similarly, in the fasted state there is a
285 substantial increase in the *Pck1* signal with 71 % of the hepatocytes positive for *Pck1*
286 (Fig. S5D). Having established this gating range, when we co-label the fed state
287 hepatocytes with both the *Pck1* and *Fasn* probes and identified that approximately 12%
288 of the hepatocytes were dual-positive (Fig. S5E). With a quantitative method in hand,
289 we determined the number of dual *Pck1*/*Fasn* positive hepatocytes relative to the single
290 positive and dual negative hepatocytes and performed euglycemic-hyperinsulinemic
291 clamps in the 24-hour fasted state and the fed state at various insulin infusion rates. We
292 also determined the relative suppression of the *Pck1* and *G6pc* mRNA in total
293 hepatocytes. Under these conditions, the fasted *Pck1* and *G6pc* mRNA expression
294 levels significantly decreased at 0.3 mU/kg/min (Fig. S5F and S5G). In contrast, fed
295 *Pck1* mRNA in the dual-positive hepatocytes was not suppressed until 2 mU/kg/min of
296 infused insulin (Fig. S5H). These data directly demonstrate that the *Fasn*/*Pck1* dual-
297 positive hepatocytes are transcriptionally insulin resistant compared to the bulk liver
298 hepatocytes.
299 Together these findings demonstrate that a subset of PP hepatocytes simultaneously
300 express both gluconeogenic and lipogenic genes in the fed state (Figs. 2, 3, S3 and
301 S4), and that isolated PP hepatocytes can also display both gluconeogenic and *de novo*
302 lipogenic activities in the fed state (Fig. 4). However, this data does not directly
303 demonstrate that individual dual-positive hepatocytes are in fact dual functional. To test

304 for this possibility, we employed single cell spatial metabolic imaging to simultaneously
305 assess both gluconeogenic and *de novo* lipogenic activities within individual
306 hepatocytes
307
308 **A subset of liver regions has higher ATP turnover in the fed state**
309 Depending upon the substrate, gluconeogenesis requires 6-10 ATP molecules per
310 molecule of glucose generated. Similarly, synthesis of palmitate from acetyl-CoA
311 requires 7 ATP and 14 NAPDH molecules. Thus, if a single hepatocyte is
312 simultaneously engaged in both gluconeogenesis and *de novo* lipogenesis, it can be
313 hypothesized that there must necessarily be a high rate of ATP turnover compared to
314 the other bulk hepatocytes. During the process of energetic addition of phosphates to
315 nucleotides or metabolites, there is an exchange of the oxygen in the phosphate with
316 the oxygen in cell water[18-21]. ATP turnover reflects the percentage of ^{16}O in ATP
317 replaced by ^{18}O after the *in vivo* administration of ^{18}O-labeled water, reflecting whole
318 cell energetics, as the exchange of ^{18}O in high energy phosphates includes ATP
319 synthesis and ATP hydrolysis, and the ^{18}O can also be exchanged with creatine kinase
320 and adenylate kinase catalyzed phosphotransfer[22,23] (Table S1). Thus, we treated mice
321 with or without ^{18}O labeled water *in vivo* coupled with spatial imaging by DESI-Cyclic
322 IMS TOF. Figure 5 shows liver sections from the fed and 24 h fasted state that were
323 either untreated (unlabeled) or treated with ^{18}O labeled water as we previously reported
324 [23]. Mass spectrometry imaging was done at 60x60 μm for the mass of normally
325 abundant m0 (unlabeled) AMP in the negative ion mode. As mouse hepatocytes are
326 polygonal and are nominally 20-30 μm in diameter, this resolution likely reflects the

327 combination of several cells[24]. Regardless, the relative amount of the m0 AMP indicated
328 a relatively low signal in the fed state but was markedly increased in the fasted state,
329 indicating a greater turnover of AMP in the fasted state (Fig. 5A). In contrast, imaging
330 for ^{18}O-labeled AMP (m0+2 AMP) demonstrated an increased signal from background
331 in both the fasted and fed states, from the mice treated with ^{18}O labeled water
332 compared to control mice livers (Fig. 5B). More importantly, the liver cross-section in the
333 fasted state showed increased intensities suggesting increased turnover relative to the
334 fed state (Fig. 5B). In contrast, m0+2 ADP fasted and fed intensities were similar over
335 each slice, suggesting turnover was similar between the fed and fasted state. The
336 increase of m0+2 ATP intensities over the liver cross-section suggested turnover was
337 increased in the fed state compared to the fasted state, which would correspond to an
338 increase in ATP generation in the fed state (Fig. 5C). As these AMP, ADP and ATP
339 measurements were done on the same slice, m0+2 ADP and m0+2 ATP pixel densities
340 can be compared to m0+2 AMP in fed state with multiple sites of overlap between m0+2
341 AMP, ADP and ATP (Fig. 5D). These results revealed several discrete pixels that
342 clearly overlapped between m0+2 AMP (red), ADP (blue) and ATP (green) (Fig. 5D).
343 The white areas indicate pixel regions with strong overlap for all three signals. These
344 data strongly indicate that a small subset of liver regions have higher rates of ATP, ADP
345 and AMP turnover in the fed state, indicating increased energetics, which might be
346 expected for Dual-Modal hepatocytes.
347
348 **A subset of hepatocytes is lipogenic and gluconeogenic**

349 To more specifically address whether an individual hepatocyte can simultaneously
350 undergo both *de novo* lipogenesis and gluconeogenesis, we next utilized metabolic
351 spatial imaging to identify the formation of m0+4 palmitate (*de novo* lipogenesis) and
352 m0+3 glucose-6-phosphate (gluconeogenesis) from a liver section of mice *in vivo* fed
353 with U[^{13}C]-glucose. m0+3 glucose-6-phosphate (3 labeled carbons) can only be formed
354 from U[^{13}C]-glucose (6 labeled carbons) when the m0+6 glucose is metabolized to a
355 m0+3 triose. The triose then goes up the gluconeogenic pathway to glucose or first
356 down the glycolytic pathway into the TCA cycle and then back up the glycolytic pathway
357 to form glucose (Fig. 6A). On the other hand, labeled palmitate can only be formed if the
358 U[^{13}C]-glucose becomes m0+3 pyruvate and then enters the TCA cycle through
359 pyruvate dehydrogenase to generate the 2-carbon labeled acetyl-CoA. Subsequent
360 metabolism and addition of these 2-carbon labeled units for fatty acid synthesis results
361 in the formation of m0+2, m0+4 etc. labeled palmitate (Fig. 6A). The dual-imaging of
362 m0+4 palmitic acid (red) and m0+3 glucose-3-phosphate (blue) by DESI MSI at 25 x 25
363 μm demonstrated the presence of pixels that were dual positive for both (pink, indicated
364 by arrows) (Fig. 6B). The same experiment was performed with MALDI MSI in a lower
365 magnification (50 x 50 μm). The ingestion of U[^{13}C]-glucose in the fed state resulted in
366 the appearance of m0+4 palmitate acid (red) and m0+3 glucose-6-phosphate (blue)
367 throughout the liver section whereas there was no detectable background labeling when
368 ingestion of unlabeled glucose in a parallel mouse (Fig. 6C). A higher magnification of
369 this MALDI image showed the presence of pixels that were dual positive for both m0+4
370 palmitic acid and m0+3 glucose-6-phosphate (pink, indicated by arrows) (Fig. 6D).
371 Since this resolution does not provide single cell information[24], we next performed mass

372 spectrometry spatial imaging at 10 μm resolution for m0+4 palmitic acid (red) and m0+3
373 glucose-6-phosphate (blue) that we co-registered with H&E staining (Fig. 6E and F). As
374 is apparent, in this imaging each pixel is smaller than the hepatocytes and with a high
375 probability it represents a single hepatocyte (Fig. 6E and F). Consistent with the lower
376 resolution image, individual hepatocytes mostly display *de novo* lipogenesis in the fed
377 state (m0+2 palmitic acid positive, red) with fewer hepatocytes positive for m0+3
378 glucose-6-phopshate (blue). However again, there were several pixels in the field that
379 are dual positive (pink), consistent with the overlap seen with ATP, ADP and AMP
380 turnover (Fig. 5) and the dual-positive hepatocytes present as measured by both
381 scRNA-seq and PrimeFlow. As these data confirm the metabolic functional duality
382 (simultaneous gluconeogenic and *de novo* lipogenic activities), we have termed these
383 as Dual-Modal hepatocytes.
384
385 **Humanized mouse liver has dual-positive spots**
386 Having established the presence of hepatocyte subsets that simultaneously express
387 both *Fasn* and *Pck1* mRNA in the fed state of mouse liver, we addressed whether dual-
388 positive hepatocytes are also present in human liver hepatocytes. As patient surgical
389 interventions can only be performed in the fasted state, it is not possible to obtain liver
390 specimens or biopsy samples from humans in the fed state. Thus, we utilized a
391 humanized mouse model in which human hepatocytes replace greater than 95 % of the
392 mouse hepatocytes and performed 10x Genomics spatial transcriptomics Visium
393 analyses on liver sections[25].Similar to the mice data, RT-qPCR for human *Fasn* showed
394 relatively low expression in the fasted state with induction in the fed state (Fig. S6A).

395 Additionally, the human *Fasn* PCR primers were unable to detect *Fasn* mRNA in wild-
396 type mouse liver, indicating no cross-reactivity. Similarly, the human *pck1* PCR primers
397 did not cross-react with mouse *Pck1* but clearly displayed the fasted state induction of
398 *Pck1* (Fig. S6B). As the Visium protocol requires a prior fixation step, we also confirmed
399 that this fixation step did not disrupt the integrity of mRNA detection by RT-qPCR (Fig.
400 S6C and D). Relative differences in the expression of the human PC marker (*CYP1A2*)
401 and PP marker (*HSD17B13*) as shown in the violin plots (Fig. S6E and S6F) enabled
402 the identification of PC spots (blue) and PP spots (red) (Fig. S6G). The violin plots for
403 *Fasn* (Fig. S6H) and *Pck1* (Fig. S6I) display the expected zonation, in particular the
404 *Pck1* mRNA in the PP hepatocytes are elevated compared to those of the PC
405 hepatocytes. The distribution of the *Fasn*/*Pck1* dual-positive spots is marked in yellow
406 with the H&E staining of the section (Fig. S6J) and with a magnified region show in
407 Figure S6K. Quantification showed 9% of the PP hepatocytes were *Fasn*/*Pck1* dual-
408 positive (Fig. S6L). These results suggest Dual-Modal hepatocytes presumable exist in
409 human hepatocytes as well.
410

411 **Dual-positive spots increase in high-fat diet fed mice liver**

412 Lastly, having established the Dual-Modal (*Fasn*/*Pck1* positive) hepatocytes that are
413 naturally insulin resistant (Fig. S4) and are gluconeogenic in the fed state, we
414 speculated that in states of insulin resistance the number of these hepatocytes might
415 increase. To test this hypothesis, we determined the number of Dual-Modal hepatocytes
416 in mice fed a normal chow diet (NCD) or a high-fat diet for 3 months (3MHFD) and used
417 the Visium platform for spatial single dot analyses. t-SNE plots showed separation

418 between NCD and 3MHFD (Fig. S7A). Graph-based clustering showed zonation
419 patterns in both NCD and 3MHFD (Fig. S7B, S7C). Based on analyses of several
420 zonation markers such as *Cyp2e1* and *Glul* for pericentral (Fig. S7D) and *Cyp2f2* and
421 *Hsd17b13* for periportal (Fig. S7E), we identified the PC (pink) and PP (blue) spots in
422 the t-SNE plot, showing clear separation (Fig. S7F). The PC and PP regions in
423 comparison with histological H&E staining are shown in Figure 7A. The presence of lipid
424 droplets in the HFD fed mice that are specifically localized to the PC hepatocytes is
425 readily observed in the magnified region shown in Figure 7B, consistent with the known
426 zonation of triglyceride accumulation[26]. The distribution of zonation markers as violin
427 plots is shown in Figures 7C and 7D. As expected for the fed state, *Fasn* mRNA was
428 expressed in both PC and PP hepatocytes in both the NCD and 3MHFD fed mice (Fig.
429 S7G). Consistent with our previous findings, *Pck1* mRNA was also present in a subset
430 of periportal hepatocytes (Fig. S7H) that overlapped with the *Fasn* dots (Fig. S7G). The
431 overlap of *Fasn* and *Pck1* mRNA positive dots in the NCD and HFD fed mice is shown
432 in Figures 7E. Quantification of the number of dots that were dual positive was
433 approximately 4 % under NCD diet but following 3 months of HFD the number of dual
434 positive dots increased to approximately 13 % (Fig. 7F). Moreover, these overlapping
435 dots primarily occurred in the PP region (Fig. 7G). These data demonstrate that long
436 term HFD results in an increase in the number of the Dual-Modal (*Fasn*/*Pck1* positive)
437 hepatocytes.
438
439 **DISCUSSION**

440 Gluconeogenesis is a fundamental metabolic process in which non-carbohydrate
441 carbon substrates such as lactate, glycerol and amino acids are used to generate
442 glucose[2,27]. In mammals' gluconeogenesis is primarily performed in the hepatocyte,
443 although kidney and intestine cells are capable of driving significant gluconeogenesis as
444 well[27-29]. In general, gluconeogenesis is inhibited in the fed state when plasma glucose
445 levels rise as a result of dietary absorption, and insulin secretion is stimulated. In the
446 fasted state, dietary derived plasma glucose levels decline, reducing insulin secretion
447 and stimulating glucagon and epinephrine release to activate hepatic gluconeogenesis
448 and glucose release to restore and maintain a normal glycemic state. Two of the key
449 gluconeogenic enzymes phosphoenolpyruvate carboxykinase (gene *Pck1*) and glucose
450 6-phosphate catalytic subunit (gene *G6pc*) are not thought to be allosterically regulated,
451 but acutely controlled at the level of gene expression through upstream transcription
452 factors that are activated by protein kinase A (i.e., CREB, HNF4α, FoxO1) signaling and
453 suppressed by insulin signaling[27].
454 Despite this generalized regulation of hepatic gluconeogenic gene expression and
455 gluconeogenic activity in the fed and fasted states, previous studies assessing
456 gluconeogenesis observed a basal level of glucose production from the liver even in the
457 fed state[6,7]. In fact, examination of numerous hyperinsulinemic-euglycemic clamp data
458 clearly shows that an insulin suppression of hepatic glucose production is never
459 zero[30,31]. This has been typically ignored and assumed to simply represent a
460 background signal. Our data suggest otherwise, as the mRNA expression and
461 transcription of lipogenic genes are essentially zero in their respective off-state (fasted),
462 whereas there is always a measurable level of gluconeogenic gene expression,

463 transcriptional activation and gluconeogenic activity in their respective off-state (fed).
464 This fed state mRNA expression of *Pck1* was confirmed by multiple, independent
465 methodologies, including targeted quantitative single cell RNAseq, smFISH, HCR RNA-
466 FISH and PrimeFlow. Moreover, PrimeFlow demonstrated the presence of both mRNA
467 for *Fasn* and *Pck1* in the same cells and HCR RNA-FISH clearly visualized the same
468 nuclei displaying transcription sites for both *Fasn* and *Pck1*. Each of these assays
469 indicated a subset of periportal hepatocytes is dual *Fasn* and *Pck1* positive in the fed
470 state.

471 Hepatocyte zonation is well established as a property of regionally distinct cellular
472 functions localized across the liver lobule, and studies in the 1980's using fasted rats
473 reported that there was a 2 to 3-fold bias of gluconeogenesis in isolated PP hepatocytes
474 relative to PC hepatocytes[14,32]. We also found an approximate 1.4-fold bias in
475 gluconeogenic activity and *Pck1* gene expression in PP versus PC hepatocytes of
476 fasted mice. However, analyses of gluconeogenic activity in the fed state, although
477 absolutely less than in the fasted state, was approximately 3.2-fold greater in PP versus
478 PC hepatocytes. In parallel, very few *Pck1* transcription sites and very low levels of
479 *Pck1* mRNA or protein were detected in fed PC hepatocytes compared to PP
480 hepatocytes. These data are consistent with a subset of PP hepatocytes being
481 responsible for the basal (fed state) level of gluconeogenesis. As such, we refer to this
482 hepatocyte subset as Dual-Modal (DM) hepatocytes.

483 The conversion of U[^{13}C]-glucose to m0+2- and m0+4-palmitate is generally
484 accepted as a direct measure of *de novo* lipogenesis that is readily detected by mass
485 spectrometry imaging[33]. However, spatial mass spectrometry imaging cannot detect

486 labeled glucose within a hepatocyte, as glucose is rapidly secreted. Instead, we
487 measured hepatocyte content of m0+3-glucose-6-phosphate derived from ingested
488 U[^{13}C]-glucose. In order for U[^{13}C]-glucose to generate m0+3-glucose-6-phosphate, the
489 U[^{13}C]-glucose must at minimum be converted by glycolysis or the pentose cycle into
490 the triose pool, which in turn can either enter the TCA cycle (pyruvate->oxaloacetate-
491 >PEP->triose-P pool) for gluconeogenesis/glyceroneogenesis, or the trioses glycerol-3-
492 phosphate and dihydroacetone phosphate recombine to form fructose-1,6-phosphate
493 and subsequently glucose-6-phosphate. Regardless of whether recycled glucose is
494 derived from the triose-P pool after traveling to the triose-P pool via glycolysis and the
495 TCA cycle or the pentose cycle and/or via the TCA cycle, our finding of the generation
496 of m0+3-glucose-6-phosphate from ingested U[^{13}C]-glucose demonstrates that in the
497 fed state, a subset of hepatocytes exhibits a simultaneous, bidirectional metabolic flow
498 up and down the glycolytic pathway. Our finding that isolated PP hepatocytes in the fed
499 state generate secreted glucose is consistent with a novel demonstration of
500 gluconeogenesis in the fed state.
501 However, these data do not rule out other metabolic pathways for the generation of
502 stable isotope labeled trioses. For example, the trioses could also contribute to
503 glyceroneogenesis that in the fed state are needed for the generation of the backbone
504 for triacylglycerol synthesis. Another more intriguing possibility is that the formation of
505 m0+3 glucose-6-phosphate in the fed state may account for previous observations
506 supporting an indirect pathway for glycogen synthesis[8-11]. After glycogen is depleted in
507 the fasted state, it can be re-synthesized in the fed state by the direct pathway (dietary
508 glucose converted to glucose-6-phosphate epimerized to glucose-1-phosphate that

509 generates UDP-glucose for direct addition to glycogen[9,11]. Alternatively, glucose but
510 also gluconeogenic substrates (i.e., amino acids) can be used to generate trioses by
511 cycling down the glycolytic pathway into the TCA cycling and then metabolized via
512 pyruvate carboxylase then PEPCK to generate triose-P which can then generate
513 glucose-6-phosphate that is then used for the re-synthesis of glycogen[8-11]. Additional
514 stable isotope flux analyses will be necessary to distinguish between these distinct
515 routes of carbohydrate flux in this unique hepatocyte subpopulation, and which likely are
516 not mutual exclusive.

517 While we observed that both normal mouse liver as well as humanized mouse livers
518 express naturally insulin resistant, Dual-Modal hepatocytes, their functions in systemic
519 physiology and pathophysiology remain to be determined. One possibility is that during
520 ingestion of ketogenic diets, glucose, although lowered, still needs to be produced. In
521 this case, Dual-Modal hepatocytes could provide a mechanism to maintain basal
522 glycemic levels necessary for survival. Pathophysiologically, high-fat diet induced insulin
523 resistance resulted in an increase in the number of Dual-Modal hepatocytes. This opens
524 up the intriguing possibility that the change in proportion of this unique hepatocyte
525 subpopulation may be an important component leading to hepatic insulin resistance.
526

527 **Limitations of the study**

528 While we have identified a subset of hepatocytes termed Dual-Modal hepatocytes
529 that could potentially explain the cause of hepatic insulin resistance based on an
530 increased number of Dual-Modal hepatocytes in high-fat diet fed mice, it is important to
531 recognize that these data do not distinguish between whether the number of Dual-

532 Modal hepatocytes increase due to proliferation of the pre-existing Dual-Modal
533 hepatocyte subpopulation and/or due to the development of insulin resistance in normal
534 hepatocytes. Future lineage tracing studies will be necessary to assess these two
535 possibilities. Also, this study does not molecularly address how an individual cell can
536 apparently undergo gluconeogenesis and *de novo* lipogenesis at the same time, as
537 these two metabolic pathways are generally assumed to be mutually exclusive with
538 each other. The three most likely possibilities are i) futile cycling throughout the parallel
539 glycolytic and gluconeogenic pathways for either periportal and/or pericentral
540 hepatocytes (dependent on degree of fasted or refed states) thereby allowing
541 substrates to flow in both directions; ii) relatively rapid oscillations between
542 gluconeogenesis and *de novo* lipogenesis, perhaps operant in Dual-Modal hepatocytes,
543 so that they are not actually occurring simultaneously; and iii) subcellular
544 compartmentalization of metabolic flux such that different regions or mitochondria within
545 an individual hepatocyte can undergo either gluconeogenesis or *de novo* lipogenesis.
546

547 **RESOURCE AVAILABLITY**

548 **Lead contact**

549 Further information and requests for resources and reagents should be directed to and
550 will be fulfilled by the lead contact, Junichi Okada (junichi.okada@einsteinmed.edu)

551 **Materials availability**

552 This study did not generate new unique reagents.

553 **Data and code availability**

554 Raw ChIP and fastq files were deposited in the National Center for Biotechnology
555 Information Gene Expression Omnibus database and are available under accession
556 numbers: GSE315776, GSE263419 (previously published targeted scRNA-seq data)
557 and GSE320372 (VISIUM). This study was conducted using only publicly available
558 software; no custom code was used.
559

560 **ACKNOWLEDGEMENTS**

561 We wish to acknowledge that the data presented in this manuscript was made possible
562 through the expertise of The Albert Einstein College of Medicine Genomics, Animal
563 Physiology, Flow Cytometry and Metabolomics Core Facilities. We are thankful to Floric
564 Slimani for the smallFish package, Licheng Wu for euglycemic-hyperinsulinemic clamp
565 studies, and Shiori Okada for data analysis. This study was supported by NIH grants
566 DK020541, DK110063, DK069861, GM007491, CA013330, AI179019, AA031412, and
567 the PhoenixBio R&D Grant.
568

569 **AUTHOR CONTRIBUTIONS**

570 JO, AL, MH, AMX, RR, SVL, TS, GJS, CE, RCS, YQ and IJK all assisted in the
571 experimental design, performance and analyses of the data presented, and writing of
572 the manuscript. LL and KS assisted in the experimental design, bioinformatic analyses
573 and editing of the manuscript. VLS, FY, MH, CE, KS and JEP supervised this project,
574 experimental design, interpretation of data and writing the manuscript.
575

576 **DECLARATION OF INTERESTS**

577 The authors declare no competing interests.

578

579 **FIGURE LEGENDS**

580 **Figure 1 *Pck1* is transcribed in hepatocytes in the fed state.** (A) Relative mRNA
581 levels of *Fasn* in fed/fasted total hepatocytes. (B) Relative mRNA levels of *Pck1* in
582 fed/fasted total hepatocytes. (C) Relative mRNA levels of *Alb* in fed/fasted total
583 hepatocytes. (D) RNAP II ChIP of *Fasn* in fed/fasted total hepatocytes. (E) RNAP II
584 ChIP of *Pck1* in fed/fasted total hepatocytes. (F) RNAP II ChIP of *Alb* in fed/fasted total
585 hepatocytes. (G) RNAP II ChIP of *Ins1* in fed/fasted total hepatocytes.

586

587 **Figure 2 *Fasn* and *Pck1* are co-expressed in a subset of periportal hepatocytes.**
588 (A) UMAP visualizations of the targeted scRNA-seq based on feeding conditions. (B)
589 UMAP visualizations based on zonation. (C) UMAP of PC zonation markers *Cyp2e1*
590 and *Gulo.* (D) UMAP of PP zonation markers *Cyp2f2* and *Hsd17b13.* (E) UMAP of *Fasn*
591 positive hepatocytes. (F) UMAP of *Pck1* positive hepatocytes (G) UMAP of dual-positive
592 hepatocytes.

593

594 **Figure 3 *Fasn* and *Pck1* are actively co-transcribed in a subset of periportal**
595 **hepatocytes.** (A) HCR RNA-FISH image of *Pck1* (magenta) and *Fasn* (green) with
596 DAPI-stained nuclei (blue) in the fed state (representative image shown). Lobules show
597 the central vein (CV) on the left and the portal vein (PV) on the right. (B) Magnified
598 images of nuclei in box in panel (A). Arrows show transcription sites (TSs) (green
599 arrow=*Fasn*, white arrow=*Pck1*, individual channel images of *Pck1* and *Fasn* are shown

600 in Figure S4A and S4B). (C) Quantitative analysis of TSs in the fed state. Lines connect
601 TS quantification between PC and PP within a lobule (N=21 lobules). Data are from 3
602 individual mice and are represented with different colors. Mean ± s.d. is indicated. *P*-
603 value was calculated by paired *t*-test, N.S. if not indicated. 627 PC nuclei, 632 PP nuclei
604 were analyzed, Scale bar, 20 um. (D) HCR-RNA FISH image of *Pck1* (magenta) and
605 *Fasn* (green) with DAPI-stained nuclei (blue) in the fasted state (representative image
606 shown). Lobules show the central vein (CV) on the left and the portal vein (PV) on the
607 right. (E) Magnified images of nuclei in box in panel (D). White arrows highlight Pck1 TS
608 (individual channel images of *Pck1* and *Fasn* are shown in Figure S4C and S4D). (F)
609 Quantitative analysis of TS in the fasted state. Lines connect TS quantification between
610 PC and PP within a lobule (N=21 lobules). Data are from 3 individual mice and are
611 represented with different colors. Mean ± s.d. is indicated. *P*-value was calculated by
612 paired *t*-test, N.S. if not indicated. 705 PC nuclei, 822 PP nuclei were analyzed, Scale
613 bar, 20 um.
614
615 **Figure 4 Periportal hepatocytes have basal pyruvate-to-glucose flux in the fed**
616 **state.** (A) *De novo* palmitate measurements using deuterated water in total hepatocytes
617 from fed (n=4) and fasted (n=4) mice. Data are presented as mean values; error bars,
618 s.d. Comparison between groups was made with unpaired, two-tailed Student's *t*-test
619 (***P < 0.001). (B) Fed and fast palmitate isotopologues derived from $^{2}H_2O$ in total
620 hepatocytes. (C) ΣM_n (average ^{13}C carbons per molecule) of glucose derived from [2,3-
621 $^{13}C_2$]-pyruvate in total hepatocytes from fed (n=3) and fasted (n=5) mice. Data are
622 presented as mean values; error bars, s.d. Comparison between groups was made with

623 unpaired, two-tailed Student's *t*-test (***P < 0.001). (D) Fed and fast glucose
624 isotopologues derived from [2,3-$^{13}C_2$]-pyruvate in total hepatocytes. (E) De novo
625 palmitate measurements using deuterated water in PC/PP hepatocytes from fed (n=4)
626 and fasted (n=4) mice. Data are presented as mean values; error bars, s.d. Comparison
627 between groups was made with unpaired, two-tailed Student's *t*-test (**P < 0.01). (F)
628 Fed and fast palmitate isotopologues derived from $^{2}H_2O$ in PC/PP hepatocytes. (G) ΣM_n
629 (average ^{13}C carbons per molecule) of glucose derived from [2,3-$^{13}C_2$]-pyruvate in
630 pericentral (PC) and periportal (PP) hepatocytes from fed and fasted mice (n=5 for PC,
631 n=6 for FastPP, n=7 for FedPP). Data are presented as mean values; error bars, s.d.
632 Comparison between groups was made with unpaired, two-tailed Student's *t*-test (***P <
633 0.001). (H) Fed and fast glucose isotopologues derived from [2,3-$^{13}C_2$]-pyruvate in
634 PC/PP hepatocytes.
635
636 **Figure 5 A subset of liver regions has higher ATP turnover in the fed state.** (A)
637 Representative DESI image of unlabeled AMP (M0) from unlabeled and 18O labeled
638 water intraperitoneal+gavage mice in the fed and fasted state. (B) Representative DESI
639 image of labeled AMP (m0+2) from unlabeled and 18O labeled water
640 intraperitoneal+gavage mice in the fed and fasted state. (C) Representative DESI image
641 of labeled ADP (m0+2) (left) and ATP-Na (m0+2) (right) from 18O labeled water
642 intraperitoneal+gavage mice in the fed and fasted state. (D) Representative DESI image
643 of labeled AMP (m0+2, red), ADP (m0+2, blue), and ATP-Na (m0+2, green) merged as
644 one image. The white areas indicate pixel regions with strong overlap for all three
645 signals.

646

647 **Figure 6 A subset of hepatocytes is lipogenic and gluconeogenic.** (A) Scheme of
648 detecting Dual-modal (DM) spots with U^{13}C glucose. (B) 25 x 25 μm DESI image of
649 U[^{13}C]-glucose labeled m0+4 Palmitic acid (red) and m0+3 Glucose-6-phosphate (blue);
650 pink represent the DM spots. White arrows highlight the DM spots. (C) Low
651 magnification MALDI image of U[^{13}C]-glucose labeled m0+4 Palmitic acid (red) and
652 m0+3 Glucose-6-phosphate (blue); pink represent the DM spots, unlabeled glucose
653 section as control. Each pixel is 50 μm. (D) High magnification MALDI image of U[^{13}C]-
654 glucose labeled m0+4 Palmitic acid (red) and m0+3 Glucose-6-phosphate (blue); pink
655 represent the DM spots. White arrows highlight the DM spots. Each pixel is 50 μm. (E)
656 High magnification of H&E staining. (F) High magnification MALDI image of U[^{13}C]-
657 glucose labeled m0+2 Palmitic acid (red) and m0+3 Glucose-6-phosphate (blue); pink
658 represent the DM hepatocytes. White arrows highlight the DM hepatocytes. Each pixel
659 is 10 μm.

660

661 **Figure 7 Dual-positive spots increase in high-fat diet fed mice liver.** (A) Spatial
662 transcriptomics image of Normal Chow Diet (NCD) fed mice and 3 Month High Fat Diet
663 (3MHFD) fed mice with Pericentral (PC)/Periportal (PP) spots highlighted. (B) A
664 representative lobule shown in a higher magnification with central vein (CV) on the left,
665 portal vein (PV) on the right. Pink spots are PP, blue spots are PC. (C) Violin plot of
666 *Cyp2e1* (pericentral (PC) marker) log normalized expression in PC/PP spots of NCD
667 and 3MHFD fed mice. (D) Violin plot of *Cyp2f2* (periportal (PP) marker) log normalized
668 expression in PC/PP spots of NCD and 3MHFD fed mice. (E) Distribution of DM spots in

669 NCD and 3MHFD fed mice; yellow spots show DM spots. (F) Quantification of DM spots
670 in NCD and 3MHFD fed mice. (G) Quantification of DM spots in PC/PP spots of NCD
671 and 3MHFD fed mice.
672
673 **Supplementary Figures**
674 **Figure S1 *G6pc* is transcribed in hepatocytes in the fed state.** (A) RNAP II ChIP of
675 *Acly* in fed/fasted total hepatocytes. (B) RNAP II ChIP of *Elovl6* in fed/fasted total
676 hepatocytes. (C) RNAP II ChIP of *G6pc* in fed/fasted total hepatocytes.
677
678 **Figure S2 *Pck1* is transcribed in periportal hepatocytes in the fed state.** (A)
679 Relative mRNA levels of *Cyp2e1* in in fed/fasted PC/PP hepatocytes. (B) Relative
680 mRNA levels of *Cyp2f2* in in fed/fasted PC/PP hepatocytes. RNAP II ChIP of *Fasn* in
681 fed/fasted PC/PP hepatocytes. (D) RNAP II ChIP of *Pck1* in fed/fasted PC/PP
682 hepatocytes. (E) RNAP II ChIP of *Alb* in fed/fasted PC/PP hepatocytes. (F) RNAP II
683 ChIP of *Ins1* in fed/fasted PC/PP hepatocytes.
684
685 **Figure S3 *Acly*, *Acaca*, *Elovl6*, and *G6pc* are co-expressed in a subset of**
686 **hepatocytes.** (A) UMAP of *Acly* positive hepatocytes. (B) UMAP of *Acaca* positive
687 hepatocytes. (C) UMAP of *Elovl6* positive hepatocytes. (D) UMAP of *G6pc* positive
688 hepatocytes.
689
690 **Figure S4 *Pck1* is actively transcribed in the fed state.** (A) HCR RNA-FISH image of
691 *Pck1* (magenta) with DAPI-stained nuclei (blue) in the fed state (representative image

692 shown). Lobules show the central vein (CV) on the left and the portal vein (PV) on the
693 right. (B) HCR RNA-FISH image *Fasn* (green) with DAPI-stained nuclei (blue) in the fed
694 state (representative image shown). Lobules show the central vein (CV) on the left and
695 the portal vein (PV) on the right. (C) HCR RNA-FISH image of *Pck1* (magenta) with
696 DAPI-stained (blue) in the fasted state (representative image shown). Lobules show the
697 central vein (CV) on the left and the portal vein (PV) on the right. (B) HCR RNA-FISH
698 image *Fasn* (green) with DAPI-stained (blue) in the fed state (representative image
699 shown). Lobules show the central vein (CV) on the left and the portal vein (PV) on the
700 right. Scale bar, 20 um.
701
702 **Figure S5 Dual-positive hepatocytes are insulin resistant in suppression of *Pck1.***
703 (A) Flow cytometry gating strategy utilizing FSC-A and SSC-A for size selection of
704 hepatocytes. (B) Background fluorescence of hepatocytes. (C) Gating of *Fasn* based on
705 fed hepatocytes. (D) Gating of *Pck1* based on fasted hepatocytes. (E) Representative
706 flow cytometry result of *Fasn*/*Pck1* in the fed state; the red quadrant shows the Dual-
707 modal (DM) hepatocytes. (F) Insulin suppression of *G6pc* mRNA expression based on
708 hyperinsulinemic-euglycemic clamps on fasted hepatocytes. (G) Insulin suppression of
709 *Pck1* mRNA expression based on hyperinsulinemic-euglycemic clamps on fasted
710 hepatocytes. (H) Insulin suppression of *Pck1* mRNA expression on DM hepatocytes
711 based on hyperinsulinemic-euglycemic clamps in the fed state.
712
713 **Figure S6 Humanized mouse liver has dual-positive spots.** (A) Relative mRNA
714 levels of human *Fasn* from fresh frozen liver tissue (mouse liver vs. humanized liver,

715 fed/fasted). (B) Relative mRNA levels of human *Pck1* from fresh frozen liver tissue
716 (mouse liver vs. humanized liver, fed/fasted). (C) Relative mRNA levels of human *Fasn*
717 from 4% PFA fixed liver sections (humanized liver). (D) Relative mRNA levels of human
718 *Pck1* from 4% PFA fixed liver sections (humanized liver). (E) Violin plot of *Cyp1a2* (PC
719 marker) log normalized expression. (F) Violin plot of *Hsd17b13* (PP marker) log
720 normalized expression. (G) Spatial Transcriptomics slide from fed mice with Pericentral
721 (PC)/Periportal (PP) spots highlighted. (H) Violin plot of *Fasn* (lipogenic gene) log
722 normalized expression. (I) Violin plot of *Pck1* (gluconeogenic gene) log normalized
723 expression. (J) Spatial Transcriptomics slide from fed mice with Dual-Modal (DM) spots
724 highlighted. (K) DM spots image with PC/PP alignment. (L) Percentage of DM spots in
725 PC/PP regions.
726
727 **Figure S7 t-SNE separates NCD and 3MHFD.** (A) t-SNE visualization of spatial
728 transcriptomics based on feeding conditions (Normal Chow Diet (NCD) and 3-Month
729 High-Fat Diet (3MHFD). (B) Spatial transcriptomics image of NCD fed mice and 3MHFD
730 fed mice with graph-based clustering highlighted. (C) t-SNE visualization of spatial
731 transcriptomics based on graph-based clustering. (D) t-SNE visualization of pericentral
732 markers *Cyp2e1* and *Glul*. (E) t-SNE visualization of periportal markers *Cyp2f2* and
733 *Hsd17b13*. (F) t-SNE visualization of spatial transcriptomics based on zonation. (G)
734 spatial transcriptomics image of *Fasn* positive spots in NCD and 3MHFD fed mice. (H)
735 spatial transcriptomics image of *Pck1* positive spots in NCD and 3MHFD fed mice.
736

737 **Table S1 Compendium of $^{18}O/^{16}O$ exchange reactions which determine ATP**

738 **turnover.**

739

740 **Table S2 Primer Sequences**

741

742 **METHODS**

743 **KEY RESOURCES TABLE**

REAGENT or RESOURCE	SOURCE	IDENTIFIER
Antibodies		
RNAPII subunit B1 (Rpb1) NTD	Cell Signaling	14958
Chemicals, peptides, and recombinant proteins		
Liberase	Sigma-Aldrich	5401127001
Digitonin	Sigma-Aldrich	D141-500MG
Percoll	Sigma-Aldrich	P4937-500ML
Critical commercial assays		
ChIP DNA Clean & Concentrator kit	Zymo Research	D5205
NEBNext® Ultra™ II DNA Library Prep Kit	New England Biolabs	E7645
HCR RNA-FISH	Molecular Instruments	V3.0 (N/A)
PrimeFlow RNA Assay Kit	Invitrogen	88-18005-204
Deposited data		
ChIP sequence	This paper, GEO	GSE315776
Targeted scRNA-seq	Okada et al[5], GEO	GSE263419
Visium (spatial transcriptomics)	This paper, GEO	GSE320372
Experimental models: Organisms/strains		
C57Bl/6J	The Jackson Lab	000664
Oligonucleotides		
Illumina® single Index Primers Set 1	New England Biolabs	E7335
Illumina® single Index Primers Set 2	New England Biolabs	E7500
See Table S2 for primer sequences	This paper	N/A
Software and algorithms		
Trim Galore	Krueger et al	https://github.com/FelixKrueger/TrimGalore, V0.6.7

Bowtie2	Langmead et al[34]	V2.4.5
Samtools	Li et al[35]	V1.6
DeepTools	Ramirez et al[36]	V3.5.1
Cell Ranger	10x Genomics	V6.0.1
Small Fish (Cellpose-SAM, big-fish)	Slimani et al	https://github.com/SmallFishGUI/small_fish_gui, V2.1.10
Space Ranger	10x Genomics	V2.0.0, V3.1.0
Other		
PicoLab Rodent Diet 20	LabDiet	5053
Rodent Diet with 60 kcal% Fat	Research Diets	D12492
Modified OSD with Macronutrient Content Similar to LabDiet 5053	Research Diets	D17011901px

744

745 **EXPERIMENTAL MODEL AND STUDY PARTICIPANT DETAILS**

746 **Animals**

747 All animal studies were conducted in accordance with protocols approved by the Albert
748 Einstein College of Medicine Institutional Animal Care and Use Committee (IACUC).
749 Unless otherwise indicated, experiments were performed using 10-14-week-old
750 C57Bl/6J wild-type male mice (The Jackson Laboratory, 000664). Spatial
751 transcriptomics studies were performed using 18-week-old mice. Animals were housed
752 in an IACUC-approved facility under ambient temperature and humidity with a 12-hour
753 light/dark cycle (lights turn on 7:00, lights turn off 19:00) and group housing. Mice had
754 free access to water and laboratory mouse chow diet (LabDiet, 5053), unless otherwise
755 specified. For high-fat diet studies, mice were fed a 60% fat diet (Research Diets,
756 D12492) beginning at 6 weeks of age for 3 months.
757 To align feeding conditions, mice were trained for 3 days to a time-restricted feeding
758 schedule by removing food at 17:00 and refeeding at 9:00 the following day (16-hour
759 fasting and 8-hour feeding) as previously described[5,12]. On the day of the experiment,

760 mice were provided food with drinking water supplemented with 20% sucrose (w/v) at
761 9:00. Fed mice were sacrificed at 13:00, corresponding to 4 hours of feeding. For fasted
762 mice, food and sucrose-containing water were removed at 13:00, drinking water was
763 replaced with regular water, and mice were fasted for 24 hours before sacrifice at 13:00
764 the following day. For pericentral/pericentral ChIP sequencing studies, mice were
765 sacrificed after 16 hours of fasting. For high-fat diet studies (and control mice), food was
766 removed at 7:00, refed at 19:00, and sacrificed at 23:00 (12-hour fasting and 4-hour
767 feeding).

768 **Humanized liver chimeric mice**

769 uPA SCID-based humanized liver chimeric mice were generated as previously
770 described and maintained with vitamin C containing chow diet (modified LabDiet 5053
771 containing 130 ppm vitamin C)[25]. Humanized liver chimeric mice were subjected to a
772 time-restricted feeding schedule modified to 10-hour fasting and 14-hour feeding.

773

774 **METHOD DETAILS**

775 **Hepatocyte Isolation**

776 Liver perfusion and hepatocyte isolation were performed under anesthesia as previously
777 described[5]. For total hepatocyte isolation, a catheter was placed in the portal vein (PV)
778 and the lower inferior vena cava (IVC) was cut for drainage. For zonated hepatocyte
779 isolation, catheters were placed in both the PV and IVC, and the perfusion line was
780 connected to the PV for periportal (PP) isolation of to the IVC for pericentral (PC)
781 isolation. Livers were perfused with pre-warmed PBS (42 °C) at 5 mL/min, then
782 switched to enzyme buffer solution (EBS, 15 mL) containing liberase (0.05 mg/mL)

783 (Sigma-Aldrich, #5401127001). For zonated hepatocyte isolation, 833 µL of 5-10mM
784 digitonin (Sigma-Aldrich, #D141-500MG) was injected via the unconnected catheter
785 (IVC for PP, PV for PC), after which the vessel was cut, and perfusion was immediately
786 resumed. Following perfusion, the liver was cut from the mouse and placed in cold
787 DMEM (without glucose) or Krebs-Henseleit (KH) buffer, gently dissociated, and filtered
788 through a 100 µm cell strainer. For liver hepatocyte purification, the cells were
789 centrifuged at 40 x *g* for 5 min at 4 °C, followed by Percoll (Sigma-Aldrich, #P4937-
790 500ML) solution (80 x *g* for 10 min at 4 °C), then washed by DMEM or KH buffer.
791 Hepatocytes were counted and assessed for viability prior to downstream applications.

792 **ChIP sequencing**

793 Fixation: Total hepatocyte (Fig. 1 and Fig. S1) and periportal/pericentral hepatocyte
794 (Fig. S2) isolation was performed on fasted and fed mice as described above with the
795 exception that all sample processing after liberase digestion was done using ice-cold
796 DBPS without calcium or magnesium (Gibco, #14190136) containing protease (Sigma,
797 #S8830) and phosphatase inhibitors (Sigma, #P5726) (referred to as DPBS buffer).
798 After final wash (see above), hepatocytes were resuspended in room temperature
799 DPBS buffer at concentration of 1 million cells/mL and formaldehyde (ThermoFisher,
800 #28908) was added to final concentration of 1%. Hepatocyte suspension was fixed at
801 room temperature for 10 min with gentle rolling. Fixation was stopped by adding glycine
802 in water (final concentration of 125 mM) containing protease and phosphatase
803 inhibitors, and hepatocytes were incubated for additional 15 min at room temperature
804 with gentle rolling. Hepatocytes were washed 1X in ice-cold DPBPS buffer, aliquoted in

805 Eppendorf tubes at 1 million cells per tube, pelleted/aspirated, and snap frozen in liquid
806 nitrogen for long-term storage at -80°C.
807 Immunoprecipitation: Immunoprecipitation reagents was prepared by washing Protein A
808 Dynabeads (ThermoFisher, #10002D) in chromatin dilution buffer (0.5% Triton X-100,
809 2mM EDTA, 20mM Tris, 150 mM NaCl in water) on DynaMag-2 (ThermoFisher,
810 #12321D) and combining with anti RNAPII subunit B1 (Rpb1) NTD rabbit monoclonal
811 antibody (Cell Signaling, #14958) at ratio of 630 µg Dynabeads to 4 µg antibody per IP
812 reaction. Dynabead-antibody mixture was pre-incubated at 4°C for 3 hours with gentle
813 rolling.
814 Sonication: Fixed-frozen hepatocyte pellets (1 million cells per IP reaction) were thawed
815 on ice and washed 1X with 500 µL cold DPBS buffer before resuspension in 500 µL
816 cold DPBS buffer with 0.5% Triton-X100 and incubation on ice for 10 min. Hepatocytes
817 were then centrifuged at 2600 xg for 5 min at 4°C, gently aspirated, and washed 1X with
818 500 µL cold tris-EDTA buffer (Sigma, #93283) containing 0.5% SDS (Sigma, #71736)
819 with protease/phosphatase inhibitors (TE-SDS buffer) before centrifuging again at 2600
820 xg for 5 min at 4°C. Supernatant was carefully aspirated, pellet was resuspended with
821 200 µL cold TE-SDS buffer, and sample was transferred to 1.5 mL Bioruptor Pico tubes
822 (Diagenode, #C30010016) on ice before sonication in 4°C water bath for 3 cycles (30
823 sec on / 30 sec off) with Easy Mode using Bioruptor Pico sonication device (Diagenode,
824 #B01080010). After sonication, sample was transferred back to 1.5 mL Eppendorf tubes
825 on ice and combined with 800 µL cold chromatin dilution buffer with
826 protease/phosphatase inhibitors (see above). Samples were centrifuged at 16,000 xg
827 for for 20 min at 4°C to remove debris and supernatant containing soluble chromatin

828 was transferred to new Eppendorf tubes on ice. DNA concentration across all samples
829 was checked using Qubit dsDNA HS kit (ThermoFisher, #Q33231) and normalized with
830 chromatin dilution buffer. For each sample, a 200 µL aliquot was collected as input and
831 a second aliquot (900 µL) was combined with 100 µL of Dynabead-antibody mixture,
832 briefly vortexed, and incubated overnight at 4°C with gentle rolling.
833 Washing: After overnight incubation, IP samples were washed in 4°C cold-room as
834 follows. Samples were placed on DynaMag-2 for 1 min, supernatant was removed and
835 discarded, 500 µL of pre-chilled wash buffer was added, and samples were rotated end-
836 over-end in cold-room for 5 min before repeating this process. Washes consisted of first
837 RIPA-140 (0.1% SDS, 1% Triton X-100, 1 mM EDTA, 10 mM Tris, 140 mM NaCl, 0.1%
838 sodium deoxycholate (Sigma, #D6750) in water), second RIPA-300 (0.1% SDS, 1%
839 Triton X-100, 1 mM EDTA, 10 mM Tris, 300 mM NaCl, 0.1% sodium deoxycholate in
840 water), third LiCl buffer (250 mM LiCl (Fisher Scientific, #L121), 0.5% Igepal ca-630 (MP
841 Biomedicals, # 198596), 1 mM EDTA, 10 mM Tris, 0.5% sodium deoxycholate in water),
842 fourth Tris-EDTA buffer (Sigma, #93283) with 0.2% Triton X-100, and fifth Tris-EDTA
843 buffer alone.
844 Elution: Wash buffer was removed, and chromatin was eluted from Dynabeads as
845 follows[37]. Briefly, 100 µL of elution buffer (1% SDS, 1 mM EDTA, 10 mM Tris in water)
846 was added to beads before vortexing and incubating at 65°C for 5 min followed by room
847 temperature incubation for 15min with vortexing every 5 min. Beads were placed on
848 DynaMag-2 for 1 min, and supernatant containing immunoprecipitated chromatin (~100
849 µL) was carefully collected and saved. Beads then underwent a second round of elution,
850 and the two supernatant collections were combined (~200 µL total).

851 RNase digestion, reverse cross-linking, and DNA purification: Input and IP samples
852 were combined with NaCl (final concentration of 160 mM) and RNase A (final
853 concentration of 20 µG/mL) (Roche, # 11119915001) and incubated at 65°C overnight
854 as previously outlined[37]. Afterwards, EDTA (final concentration of 5 mM) and proteinase
855 K (final concentration 200 µG/mL) (Invitrogen, # 100005393) were added, and samples
856 were incubated at 45°C for 2 h. Finally, input and IP DNA was purified using ChIP DNA
857 Clean & Concentrator kit (Zymo Research, #D5205) according to manufacturer's
858 guidelines, and DNA concentration was quantified using Qubit dsDNA HS kit. Fraction
859 of purified input DNA was run on agarose gel to assess fragmentation pattern (~100-
860 500 bp).
861 Library preparation, sequencing, and data processing: Library preparation was
862 performed using NEBNext® Ultra™ II DNA Library Prep Kit for Illumina® (New England
863 Biolabs, #E7645) according to manufacturer's guidelines with NEBNext® Multiplex
864 Oligos for Illumina® single Index Primers Set 1 and Set 2 (New England Biolabs,
865 #E7335 and #E7500). Premade libraries were sent to Novogene for sequencing using
866 NovaSeq paired-end sequencing at 150 base pairs per read (PE150). Raw fastq files
867 were first processed to remove adapter sequences and low-quality bases using Trim
868 Galore (v0.6.7) with "--stringency 5". Trimmed reads were then aligned to mm10
869 reference genome using bowtie2 (v2.4.5) with default parameters[34]. The resulting SAM
870 files were converted to BAM files using samtools (v1.6) view with "-f 2 -q 10"[35].
871 Duplicates were removed using samtools rmdup. Coverage tracks were generated
872 using the bamCoverage tool from the deepTools (v3.5.1) suite with the "--extendReads -
873 -normalizeUsing CPM" option[36]. Input normalization was performed using log2 ratio and

874 bin size set to 5 with bigwigCompare from deepTools. Normalized BigWig files were
875 visualized using Integrative Genomics Viewer (IGV)[38]. Total hepatocyte gene tracks
876 (Fig. 1 and Fig. S1) represent IP over input signal; periportal/pericentral hepatocyte
877 gene tracks (Fig. S2) represent IP signal alone since input signal was negligible in
878 previous experiments.

879 **RNA isolation and quantitative PCR (RT-qPCR)**

880 Total RNA isolation from isolated hepatocytes was done using the RNeasy mini kit
881 (Qiagen, #74106) in combination with TRIzol (Invitrogen, #15596026) according to the
882 manufacture's protocol. cDNA was synthesized using SuperScript IV VILO (Invitrogen,
883 #11756050) and RT-qPCR was performed using PowerUp SYBR Green Master Mix
884 (Applied Biosystems, #A25778) on a QuantStudio 6 system (Applied Biosystems).
885 Relative gene expression was determined by the ΔΔCt method and normalized to *Ppib*.
886 Primer sequences are listed in Table S2.

887 **Targeted Single-cell RNA sequencing (targeted scRNA-seq)**

888 To characterize dual-modal hepatocytes, we analyzed a publicly available targeted
889 single-cell RNA sequencing (scRNA-seq) dataset covering 61 specific genes[5]. The
890 panel consisted of pericentral and periportal hepatocyte markers, general parenchymal
891 and non-parenchymal cell markers, as well as genes involved in gluconeogenesis,
892 lipogenesis, bile acid synthesis, and several secreted hepatokines. Raw FASTQ files
893 were obtained from the NCBI Gene Expression Omnibus (GEO; accession no.
894 GSE263419). Gene expression levels were quantified using Cell Ranger (v.6.0.1; 10x
895 Genomics) in targeted gene expression mode. Positive cells were defined by applying

896 thresholds determined via ridge plot analysis and compared with RT-qPCR results as
897 previously described[5].

898 **HCR RNA-FISH**

899 Livers were fixed in 4% paraformaldehyde (PFA) for 3 hours, cryoprotected in PFA + 30
900 % sucrose for overnight, embedded in OCT, and tissue blocks were kept at -80 °C until
901 sectioning. After sectioned at 8-10 μm thickness, the sections were post-fixed,
902 permeabilized with ethanol, and treated with proteinase K prior to hybridization as
903 previously described[5]. HCR RNA-FISH probes (Molecular Instruments) targeting *Pck1*
904 (B3), *Fasn* (B1), and *Glul* (B2) were hybridized overnight at 37 °C (0.4 pmol of each
905 probe set/100 uL). Once excess probes were removed, the amplification stage was
906 performed according to the manufacture's protocol for 12 hours (B3=546, B1=647,
907 B2=488, 6 pmol each of hairpin/100 uL)[39]. Sections were then washed, counterstained
908 with DAPI, and mounted with antifade medium. Images were acquired on an upright,
909 wide-field Olympus BX- 63 Microscope equipped with a Super Apochromatic objective
910 lens (60×/1.35 N.A., Pixel size (x,y) = 107.5 nm, z-step = 300nm). MetaMorph software
911 (Molecular Devices, v7.10.1.161) was used for controlling microscope automation and
912 image acquisition. Pericentral hepatocytes were identified by *Glul* expression, and
913 periportal hepatocytes were identified by the bile duct-associated morphology. Liver
914 lobule images were taken by taking sequential images and processed on FIJI (v2.16.0).
915 Transcription site analysis in hepatic lobules was performed using SmallFish (v2.1.10),
916 a python implementation of FishQuant[40]. Cell segmentation was performed in 2D using
917 Cellpose (https://github.com/MouseLand/cellpose); and spot detection was performed
918 via big-fish package (https://github.com/fish-quant/big-fish).

919 **Stable isotope tracing analyses**

920 For pyruvate-to glucose tracing experiments, isolated hepatocytes ($1x10^5$ cells) were
921 incubated in KH buffer containing 1 mM [2,3-$^{13}C_2$] sodium pyruvate or unlabeled
922 pyruvate, 1 mM sodium lactate, 2 mM L-glutamine, and 1 mM BSA-conjugated palmitic
923 acid at 37 °C for 1 hour. 200 µL of the media was extracted with methanol containing 2-
924 deoxyglucose, centrifuged (13,100 × *g*, 10 min, 4 °C), and the supernatant was dried
925 under gentle nitrogen flow. Samples were then reacted with hydroxylanmine followed by
926 acetic anhydride as previously described[5]. After reconstitution in ethyl acetate, the
927 samples were analyzed by gas chromatography mass spectrometry (GC (7890)-MS
928 (5975C), Agilent) in chemical ionization (CI) mode using methane as the CI gas.
929 Mass isotopologue distributions were analyzed using MassHunter software (Agilent)
930 and corrected for natural isotope abundance. Glucose isotopologues are reported as
931 molar fractions (M0–M6). The sum of all isotopologues of the molecules, m_i (where i = 1
932 to 6), is equal to 1 or 100%. The labelled isotopologue fractions consist of a distribution
933 not affected by the dilution with unlabeled compounds, reported as $m_i/\Sigma m_i$, in percent.
934 The enrichment ΣM_n is the weighted sum of the labelled species ($\Sigma Mn = 1*M_1 + 2*M_2 +$
935 $3*M_3 + 4*M_4 + 5*M_5 + 6*M_6$) = average number of ^{13}C carbons/molecule as previously
936 reported[5].

937 For *in vivo* deuterium labeling, mice were subjected to time-restricted feeding as
938 described above. For fed conditions, mice received an intraperitoneal (IP) injection of
939 0.9% NaCl in deuterated water (30 µL/g body weight) at 07:00, after which drinking
940 water was replaced with 6% ^2H_2O. Chow and 6 % ^2H_2O with 20 % sucrose (w/v) were
941 provided at 09:00, and mice were sacrificed at 13:00. For fasted conditions, mice were

942 fed chow and sucrose water (without $^{2}H_2O$) from 09:00 to 13:00, fasted for 24 h, injected
943 with $^{2}H_2O$ and regular drinking water was replaced with 6 % $^{2}H_2O$ water at 07:00 the
944 following day, and sacrificed at 13:00. Lipids were extracted from isolated hepatocytes
945 ($1x10^6$ cells) following alkaline saponification in 1 M NaOH in 70 % ethanol in water with
946 heptadecanoic acid (C17:0) as an internal standard. Extracted fatty acids were
947 derivatized with BSTFA and analyzed by GC-MS (Agilent) with a DB-5MS column.
948 Palmitate deuterium enrichment was quantified from the m/z 313 fragment and
949 calculated. The total labeled fraction of palmitate was calculated with fraction
950 enrichment. The total palmitate was calculated relative to the concentration of
951 heptadecanoic acid. The newly synthesized palmitate was calculated with the function:
952 Newly synthesized palmitate = Total palmitate * total fraction of labeled
953 palmitate/deuterium enrichment in plasma/tissue weight.

954 **^{18}O water labeling in vivo**

955 Mice were subjected to time-restricted feeding as described above. In both fed and
956 fasted conditions, the mice were gavage with ^{18}O water or regular water at 12:48,
957 received IP injection of ^{18}O water or regular water at 12:53, then sacrificed at 13:00. The
958 liver was rinsed with 150 mM ammonium acetate before frozen in pre-chilled
959 isopentane. A 20 um thickness of tissue section was used for DESI imaging. The slide
960 was analyzed with a Waters Cyclic Ion Mobility-Mass Spectrometry (Cyclic-iMS).
961 The slide was placed in desiccator for about half an hour before loading into DESI
962 stage. The solvent was methanol:water=60:40(v:v) with 200ng/mL LeuEnk. The flow
963 rate was set to 2 μL/min. The resolution was set to 60um with 300 μm/sec. The mass

964 range was set to 50 – 1200 m/z, and the mobility was set to 1 pass with TW ramp of
965 TOF settings are 16 – 28 V/ms.

966 **DESI and MALDI metabolic spatial imaging**

967 Mice were subjected to time-restricted feeding as described above. On the day of the
968 experiment, mice were provided with D17011901px (Modified OSD with Macronutrient
969 Content Similar to LabDiet 5053) with $^{13}C_6$ glucose or unlabeled glucose (for 1 g of
970 premix, 1.31 g of glucose was added) at 9:00. Mice were then sacrificed at 13:00,
971 corresponding to 4 hours of feeding, and the liver was frozen in pre-chilled isopentane.
972 For DESI analysis, the slices were sectioned into 20um thickness. The ^{13}C samples was
973 analyzed with DESI-Xevo TQ absolute MS (Waters). The solvent was
974 methanol:water=80:20(v:v) with 200ng/mL LeuEnk with a flow rate of 1.2ul/mL and was
975 scanned with 25 x 25 um spatial resolution. The metabolites and their isotopolgues was
976 analyzed in the negative multiple reaction monitoring (MRM) mode. The data was
977 processed with HDI software (Waters).

978 **PrimeFlow**

979 After isolating hepatocytes as described above, the hepatocytes went through the
980 PrimeFlow (Invitrogen, #88-18005-204) protocol based on the manufacturer's
981 instructions with minor modifications. Briefly, hepatocytes were fixed using PrimeFlow
982 RNA Fixation Buffers. Cells were then permeabilized in PrimeFlow RNA
983 Permeabilization Buffer supplemented with RNase inhibitors, followed by a second
984 fixation step. After washing, cells were hybridized with target-specific RNA probe sets
985 diluted in PrimeFlow RNA Target Probe Diluent for 2 hours at 40 °C. Samples were
986 washed in PrimeFlow RNA Wash Buffer containing RNase inhibitor and stored

987 overnight at 2-8 °C in the dark. On the following day, signal amplification was performed
988 through sequential incubations with PreAmp Mix, Amp Mix, and fluorescently labeled
989 probes, each at 40 °C, with intervening washes according to the manufacturer's
990 instructions. Following the final labeling step, cells were washed, resuspended in
991 PrimeFlow RNA Storage Buffer and analyzed on BD FACSAria III. All centrifugation
992 steps were done at 800 × *g* unless otherwise specified.

993 **Hyperinsulinemic-euglycemic clamp experiments**

994 Hyperinsulinemic-euglycemic clamp studies were performed in conscious, unrestrained
995 mice. Briefly, mice were surgically implanted with catheters in the jugular vein for
996 infusions and the carotid artery for blood sampling. After recovering for at least 3 days
997 following surgery, the mice were subjected to time-restricted feeding as described
998 above. On the day of the experiment, catheters were connected to infusion lines, and
999 basal blood glucose was measured from the arterial blood using a glucometer.
1000 Continuous insulin was infused at the indicated rates and maintained for 2 hours. Blood
1001 glucose was clamped at 150 mg/dL by a variable infusion of 20% glucose solution,
1002 adjusted based on blood glucose measurements every 10-20 minutes. At the end of the
1003 clamp, liver perfusion for total hepatocyte isolation was performed.

1004 **Spatial Transcriptomics**

1005 For high-fat diet studies, fresh frozen mouse livers were embedded in Neg-50 and
1006 stored at -80 °C until sectioning. After sectioned at 10 μm thickness, **s**ections were
1007 adhered to capture areas by brief warming onto Visium v1 slides (10x Genomics). For
1008 humanized liver studies, livers were fixed in 4% paraformaldehyde (PFA) for 3 hours,
1009 cryoprotected in PFA + 30 % sucrose for overnight, embedded in OCT, and tissue

1010 blocks were kept at -80 °C until sectioning. After sectioned at 10 μm thickness, Visium
1011 v2 (prepared with CytAssist) was performed using the CytAssist instrument. For both
1012 studies, the sample preparation was performed according to the manufacturer's
1013 guidelines. Briefly, tissue sections were stained with hematoxylin and eosin (H&E),
1014 imaged using a brightfield microscope for histological reference and spatial registration.
1015 RNA capture, reverse transcription, second-strand synthesis, cDNA amplification, and
1016 library construction were performed. Libraries were indexed, quality-controlled, and
1017 sequenced on an Illumina platform using paired-end sequencing. Raw sequencing data
1018 were processed using Space Ranger (v2.0.0 for high-fat diet studies with reference
1019 genome: mm10-2020-A, v3.1.0 for humanized liver studies with reference genome:
1020 GRCh38-2020-A, 10x Genomics) to align reads to the reference genome and generate
1021 spatial gene expression matrices. Spatial alignment was performed using H&E images,
1022 and downstream analyses were conducted using standard single-cell and spatial
1023 transcriptomics workflows.

1024 **QUANTIFICATION AND STATISTICAL ANALYSIS**

1025 Excel (v16.101.3), Prism (v10.6.1) GraphPad Software, were used for data processing,
1026 analyses, and graph productions in the experiments. All data are presented as the
1027 mean +/- standard deviation unless otherwise noted. Student's *t*-test with unpaired two-
1028 tailed p values of *$p<0.05$, **$p<0.01$, and ***$p<0.001$ was considered statistically
1029 significant when comparing two groups. (N.S.=not statistically significant).
1030 Figures/Images were created by Powerpoint (v16.101.3), IGV (v2.19.7), Loupe Browser
1031 (v9.0.0), FIJI (v2.16.0), QuPath (v0.6.0) and Adobe Illustrator (v28.1).
1032

1033 **REFERENCES**

1034 1 Ben-Moshe, S. & Itzkovitz, S. Spatial heterogeneity in the mammalian liver. *Nat*
1035 *Rev Gastroenterol Hepatol* **16**, 395-410 (2019). https://doi.org:10.1038/s41575-
1036 019-0134-x
1037 2 Martini, T., Naef, F. & Tchorz, J. S. Spatiotemporal Metabolic Liver Zonation and
1038 Consequences on Pathophysiology. *Annu Rev Pathol* **18**, 439-466 (2023).
1039 https://doi.org:10.1146/annurev-pathmechdis-031521-024831
1040 3 Halpern, K. B. *et al.* Single-cell spatial reconstruction reveals global division of
1041 labour in the mammalian liver. *Nature* **542**, 352-356 (2017).
1042 https://doi.org:10.1038/nature21065
1043 4 Rosenberger, F. A. *et al.* Spatial single-cell mass spectrometry defines zonation
1044 of the hepatocyte proteome. *Nat Methods* **20**, 1530-1536 (2023).
1045 https://doi.org:10.1038/s41592-023-02007-6
1046 5 Okada, J. *et al.* Spatial hepatocyte plasticity of gluconeogenesis during the
1047 metabolic transitions between fed, fasted and starvation states. *Nat Metab* **7**,
1048 1073-1091 (2025). https://doi.org:10.1038/s42255-025-01269-y
1049 6 Sasse, D., Katz, N. & Jungermann, K. Functional heterogeneity of rat liver
1050 parenchyma and of isolated hepatocytes. *FEBS Lett* **57**, 83-88 (1975).
1051 https://doi.org:10.1016/0014-5793(75)80157-8
1052 7 Wagle, S. R., Ingebretsen, W. R. & Sampson, L. Studies on gluconeogenesis
1053 and stimulation of glycogen and protein synthesis in isolated hepatocytes in
1054 alloxan diabetic, normal fed and fasted animals. *Acta Diabetol Lat* **12**, 185-198
1055 (1975). https://doi.org:10.1007/BF02581299
1056 8 Bartels, H., Vogt, B. & Jungermann, K. Glycogen synthesis via the indirect
1057 gluconeogenic pathway in the periportal and via the direct glucose utilizing
1058 pathway in the perivenous zone of perfused rat liver. *Histochemistry* **89**, 253-260
1059 (1988). https://doi.org:10.1007/BF00493149
1060 9 Petersen, M. C., Vatner, D. F. & Shulman, G. I. Regulation of hepatic glucose
1061 metabolism in health and disease. *Nat Rev Endocrinol* **13**, 572-587 (2017).
1062 https://doi.org:10.1038/nrendo.2017.80
1063 10 Coelho, M. *et al.* Enrichment of hepatic glycogen and plasma glucose from
1064 H(2)(18) O informs gluconeogenic and indirect pathway fluxes in naturally
1065 feeding mice. *NMR Biomed* **36**, e4837 (2023). https://doi.org:10.1002/nbm.4837
1066 11 Adeva-Andany, M. M., Gonzalez-Lucan, M., Donapetry-Garcia, C., Fernandez-
1067 Fernandez, C. & Ameneiros-Rodriguez, E. Glycogen metabolism in humans.
1068 *BBA Clin* **5**, 85-100 (2016). https://doi.org:10.1016/j.bbacli.2016.02.001
1069 12 Youn, D. Y. *et al.* The Mediator complex kinase module is necessary for fructose
1070 regulation of liver glycogen levels through induction of glucose-6-phosphatase
1071 catalytic subunit (G6pc). *Mol Metab* **48**, 101227 (2021).
1072 https://doi.org:10.1016/j.molmet.2021.101227
1073 13 Core, L. & Adelman, K. Promoter-proximal pausing of RNA polymerase II: a
1074 nexus of gene regulation. *Genes Dev* **33**, 960-982 (2019).
1075 https://doi.org:10.1101/gad.325142.119

1076 14 Chen, K. S. & Katz, J. Zonation of glycogen and glucose syntheses, but not
1077 glycolysis, in rat liver. *Biochem J* **255**, 99-104 (1988).
1078 https://doi.org:10.1042/bj2550099
1079 15 Quistorff, B. Gluconeogenesis in periportal and perivenous hepatocytes of rat
1080 liver, isolated by a new high-yield digitonin/collagenase perfusion technique.
1081 *Biochem J* **229**, 221-226 (1985). https://doi.org:10.1042/bj2290221
1082 16 Droin, C. *et al.* Space-time logic of liver gene expression at sub-lobular scale. *Nat*
1083 *Metab* **3**, 43-58 (2021). https://doi.org:10.1038/s42255-020-00323-1
1084 17 Henning, A. L., Sampson, J. N. B. & McFarlin, B. K. Measurement of Low-
1085 Abundance Intracellular mRNA Using Amplified FISH Staining and Image-Based
1086 Flow Cytometry. *Curr Protoc Cytom* **76**, 7 46 41-47 46 48 (2016).
1087 https://doi.org:10.1002/0471142956.cy0746s76
1088 18 Zeleznikar, R. J. & Goldberg, N. D. Kinetics and compartmentation of energy
1089 metabolism in intact skeletal muscle determined from 18O labeling of metabolite
1090 phosphoryls. *J Biol Chem* **266**, 15110-15119 (1991).
1091 19 Goldberg, N. D., Ames, A. A., 3rd, Gander, J. E. & Walseth, T. F. Magnitude of
1092 increase in retinal cGMP metabolic flux determined by 18O incorporation into
1093 nucleotide alpha-phosphoryls corresponds with intensity of photic stimulation. *J*
1094 *Biol Chem* **258**, 9213-9219 (1983).
1095 20 Walseth, T. F., Gander, J. E., Eide, S. J., Krick, T. P. & Goldberg, N. D. 18O
1096 labeling of adenine nucleotide alpha-phosphoryls in platelets. Contribution by
1097 phosphodiesterase-catalyzed hydrolysis of cAMP. *J Biol Chem* **258**, 1544-1558
1098 (1983).
1099 21 Dawis, S. M. *et al.* Adenosine triphosphate utilization rates and metabolic pool
1100 sizes in intact cells measured by transfer of 18O from water. *Biophys J* **55**, 79-99
1101 (1989). https://doi.org:10.1016/S0006-3495(89)82782-1
1102 22 Zeleznikar, R. J. *et al.* Evidence for compartmentalized adenylate kinase
1103 catalysis serving a high energy phosphoryl transfer function in rat skeletal
1104 muscle. *J Biol Chem* **265**, 300-311 (1990).
1105 23 Tang, Y. *et al.* TIGAR deficiency enhances skeletal muscle thermogenesis by
1106 increasing neuromuscular junction cholinergic signaling. *Elife* **11** (2022).
1107 https://doi.org:10.7554/eLife.73360
1108 24 Hall, A. *et al.* Transaminase abnormalities and adaptations of the liver lobule
1109 manifest at specific cut-offs of steatosis. *Sci Rep* **7**, 40977 (2017).
1110 https://doi.org:10.1038/srep40977
1111 25 Sugahara, G., Ishida, Y., Sun, J., Tateno, C. & Saito, T. Art of Making Artificial
1112 Liver: Depicting Human Liver Biology and Diseases in Mice. *Semin Liver Dis* **40**,
1113 189-212 (2020). https://doi.org:10.1055/s-0040-1701444
1114 26 Seubnooch, P. *et al.* Characterisation of hepatic lipid signature distributed across
1115 the liver zonation using mass spectrometry imaging. *JHEP Rep* **5**, 100725
1116 (2023). https://doi.org:10.1016/j.jhepr.2023.100725
1117 27 Hatting, M., Tavares, C. D. J., Sharabi, K., Rines, A. K. & Puigserver, P. Insulin
1118 regulation of gluconeogenesis. *Ann N Y Acad Sci* **1411**, 21-35 (2018).
1119 https://doi.org:10.1111/nyas.13435

1120 28 Sahoo, B., Srivastava, M., Katiyar, A., Ecelbarger, C. & Tiwari, S. Liver or kidney:
1121 Who has the oar in the gluconeogenesis boat and when? *World J Diabetes* **14**,
1122 1049-1056 (2023). https://doi.org:10.4239/wjd.v14.i7.1049
1123 29 Mutel, E. *et al.* Control of blood glucose in the absence of hepatic glucose
1124 production during prolonged fasting in mice: induction of renal and intestinal
1125 gluconeogenesis by glucagon. *Diabetes* **60**, 3121-3131 (2011).
1126 https://doi.org:10.2337/db11-0571
1127 30 Edgerton, D. S. *et al.* Insulin's direct hepatic effect explains the inhibition of
1128 glucose production caused by insulin secretion. *JCI Insight* **2**, e91863 (2017).
1129 https://doi.org:10.1172/jci.insight.91863
1130 31 Buettner, C. *et al.* Severe impairment in liver insulin signaling fails to alter hepatic
1131 insulin action in conscious mice. *J Clin Invest* **115**, 1306-1313 (2005).
1132 https://doi.org:10.1172/JCI23109
1133 32 Tosh, D., Alberti, G. M. & Agius, L. Glucagon regulation of gluconeogenesis and
1134 ketogenesis in periportal and perivenous rat hepatocytes. Heterogeneity of
1135 hormone action and of the mitochondrial redox state. *Biochem J* **256**, 197-204
1136 (1988). https://doi.org:10.1042/bj2560197
1137 33 Buglakova, E. *et al.* Spatial single-cell isotope tracing reveals heterogeneity of de
1138 novo fatty acid synthesis in cancer. *Nat Metab* **6**, 1695-1711 (2024).
1139 https://doi.org:10.1038/s42255-024-01118-4
1140 34 Langmead, B. & Salzberg, S. L. Fast gapped-read alignment with Bowtie 2. *Nat*
1141 *Methods* **9**, 357-359 (2012). https://doi.org:10.1038/nmeth.1923
1142 35 Li, H. A statistical framework for SNP calling, mutation discovery, association
1143 mapping and population genetical parameter estimation from sequencing data.
1144 *Bioinformatics* **27**, 2987-2993 (2011).
1145 https://doi.org:10.1093/bioinformatics/btr509
1146 36 Ramirez, F. *et al.* deepTools2: a next generation web server for deep-sequencing
1147 data analysis. *Nucleic Acids Res* **44**, W160-165 (2016).
1148 https://doi.org:10.1093/nar/gkw257
1149 37 Sullivan, A. E. & Santos, S. D. M. An Optimized Protocol for ChIP-Seq from
1150 Human Embryonic Stem Cell Cultures. *STAR Protoc* **1**, 100062 (2020).
1151 https://doi.org:10.1016/j.xpro.2020.100062
1152 38 Robinson, J. T. *et al.* Integrative genomics viewer. *Nat Biotechnol* **29**, 24-26
1153 (2011). https://doi.org:10.1038/nbt.1754
1154 39 Choi, H. M. *et al.* Programmable in situ amplification for multiplexed imaging of
1155 mRNA expression. *Nat Biotechnol* **28**, 1208-1212 (2010).
1156 https://doi.org:10.1038/nbt.1692
1157 40 Imbert, A. *et al.* FISH-quant v2: a scalable and modular tool for smFISH image
1158 analysis. *RNA* **28**, 786-795 (2022). https://doi.org:10.1261/rna.079073.121
1159

Figure 1 – *Pck1* is transcribed in hepatocytes the fed state

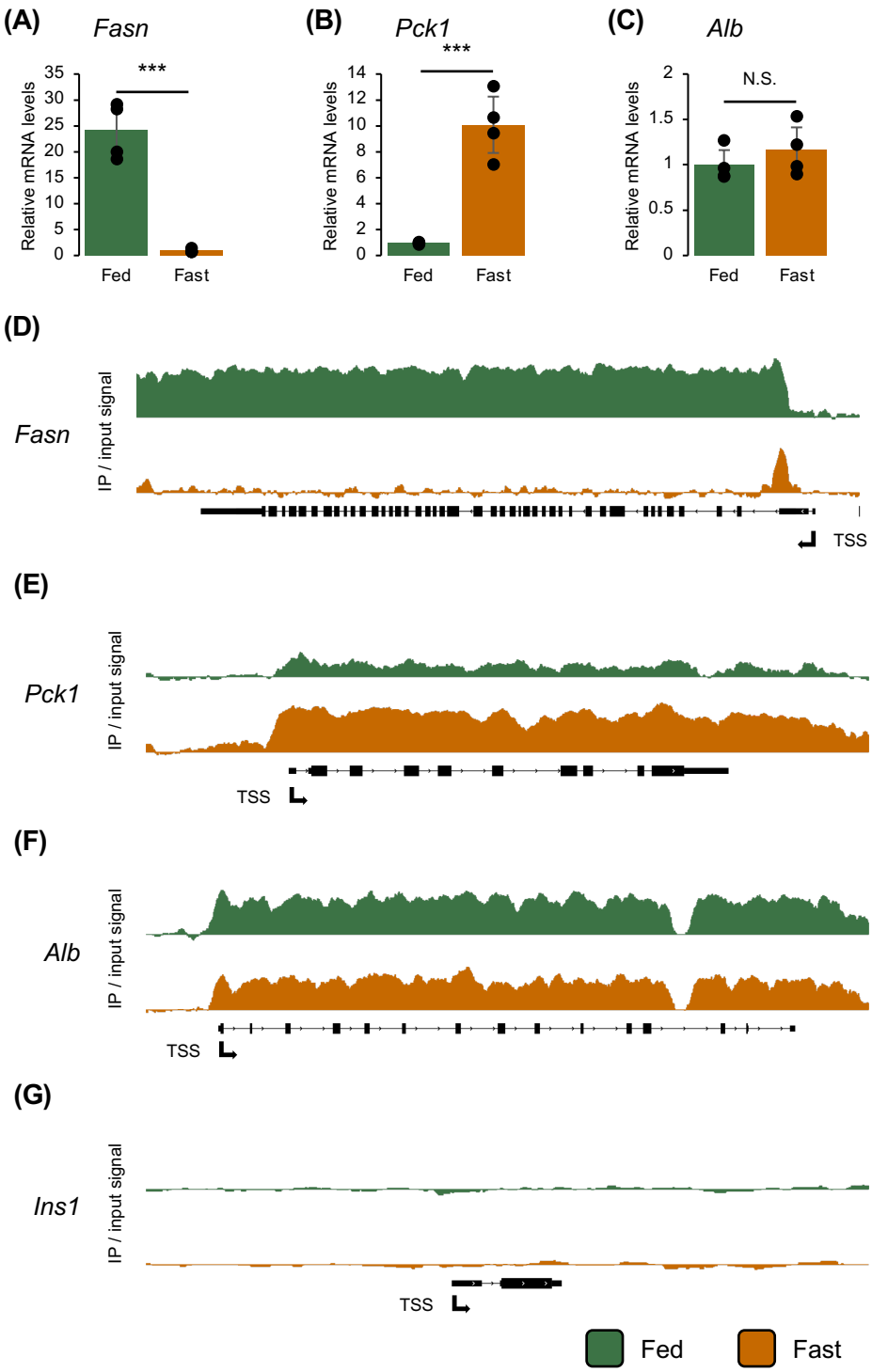

Figure 2 – *Fasn* and *Pck1* are co-expressed in a subset of periportal hepatocytes

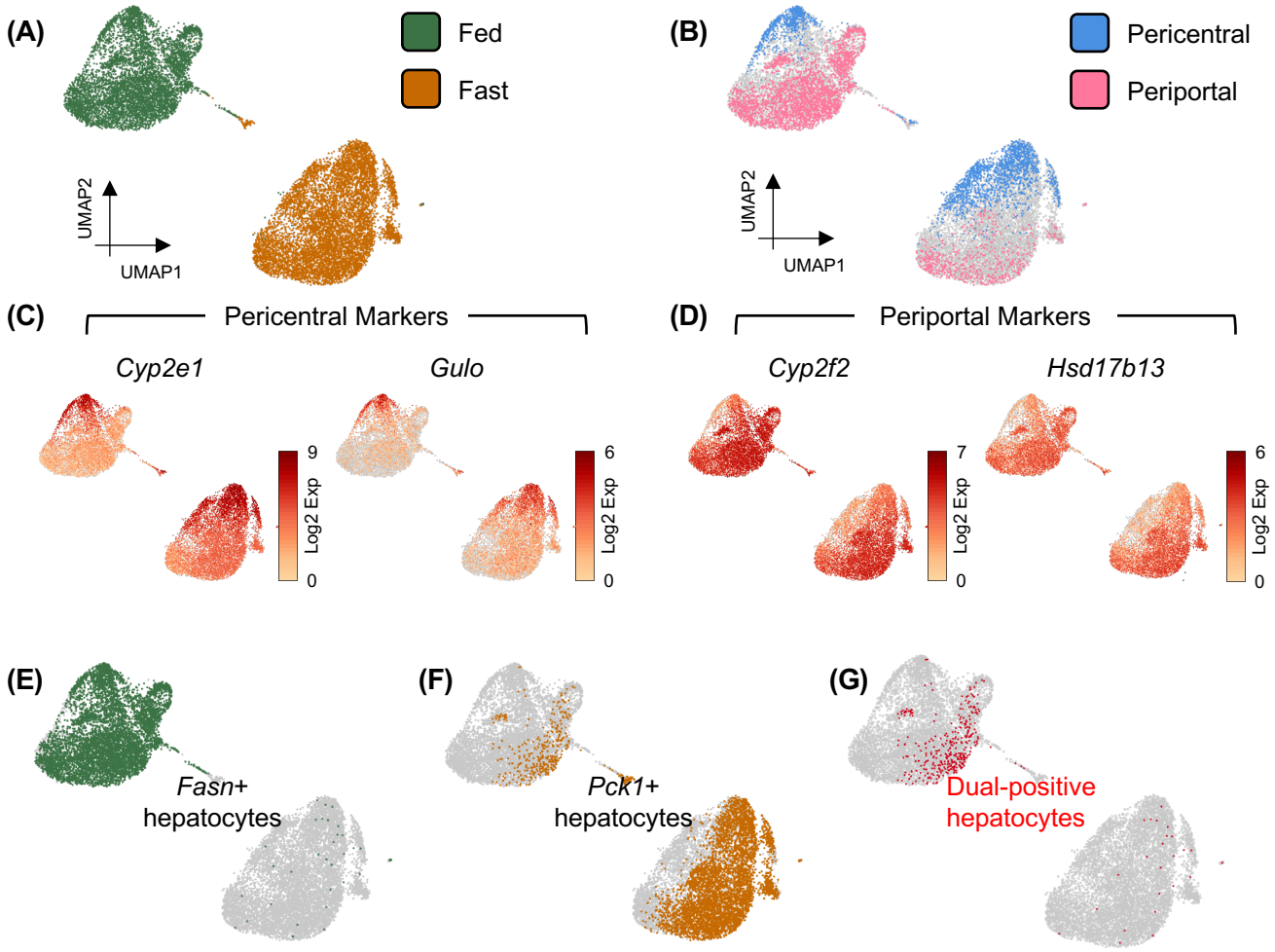

Figure 3 – *Fasn* and *Pck1* are actively co-transcribed in a subset of periportal hepatocytes

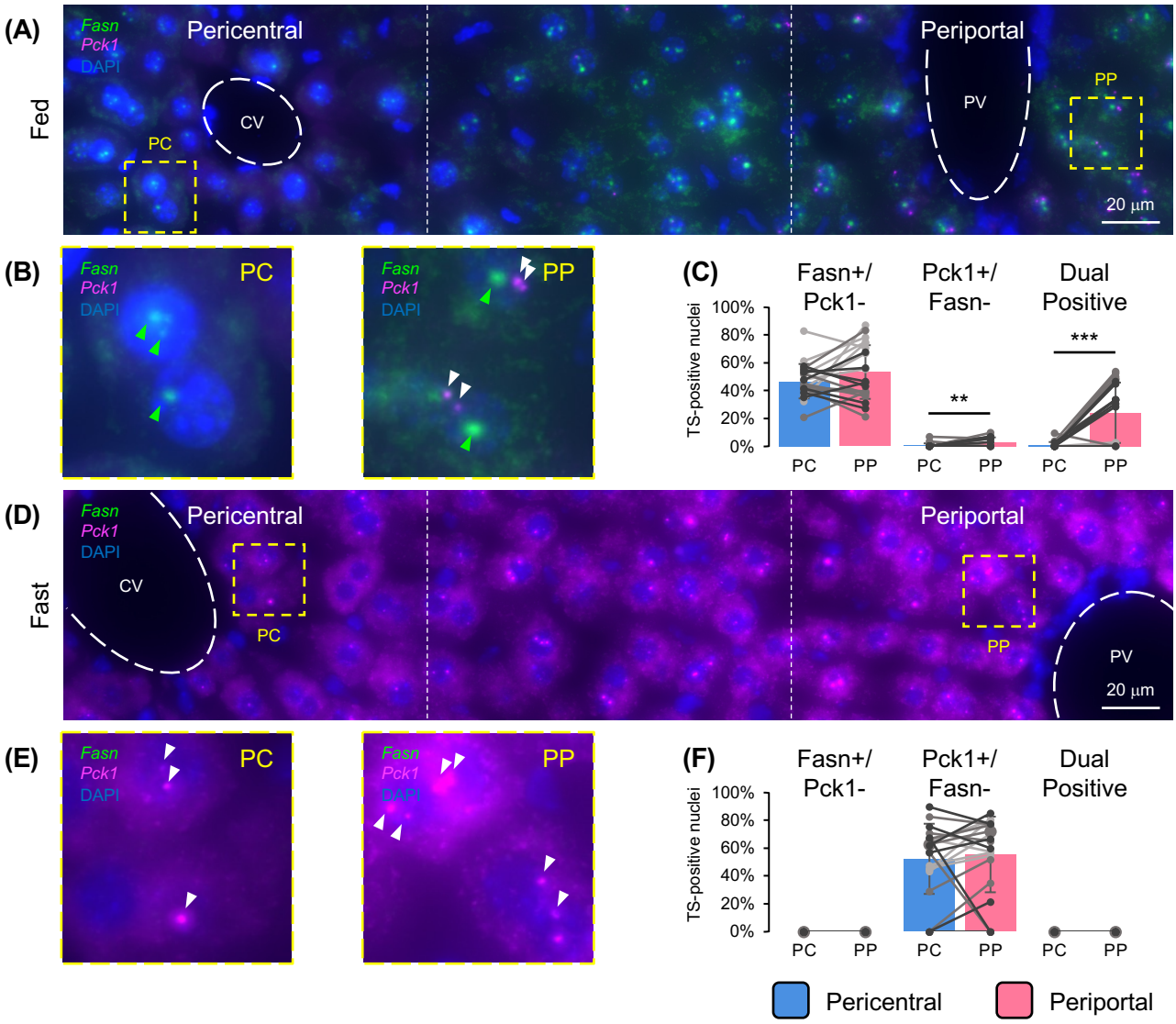

Figure 4 – Periportal hepatocytes have basal pyruvate-to-glucose flux in the fed state

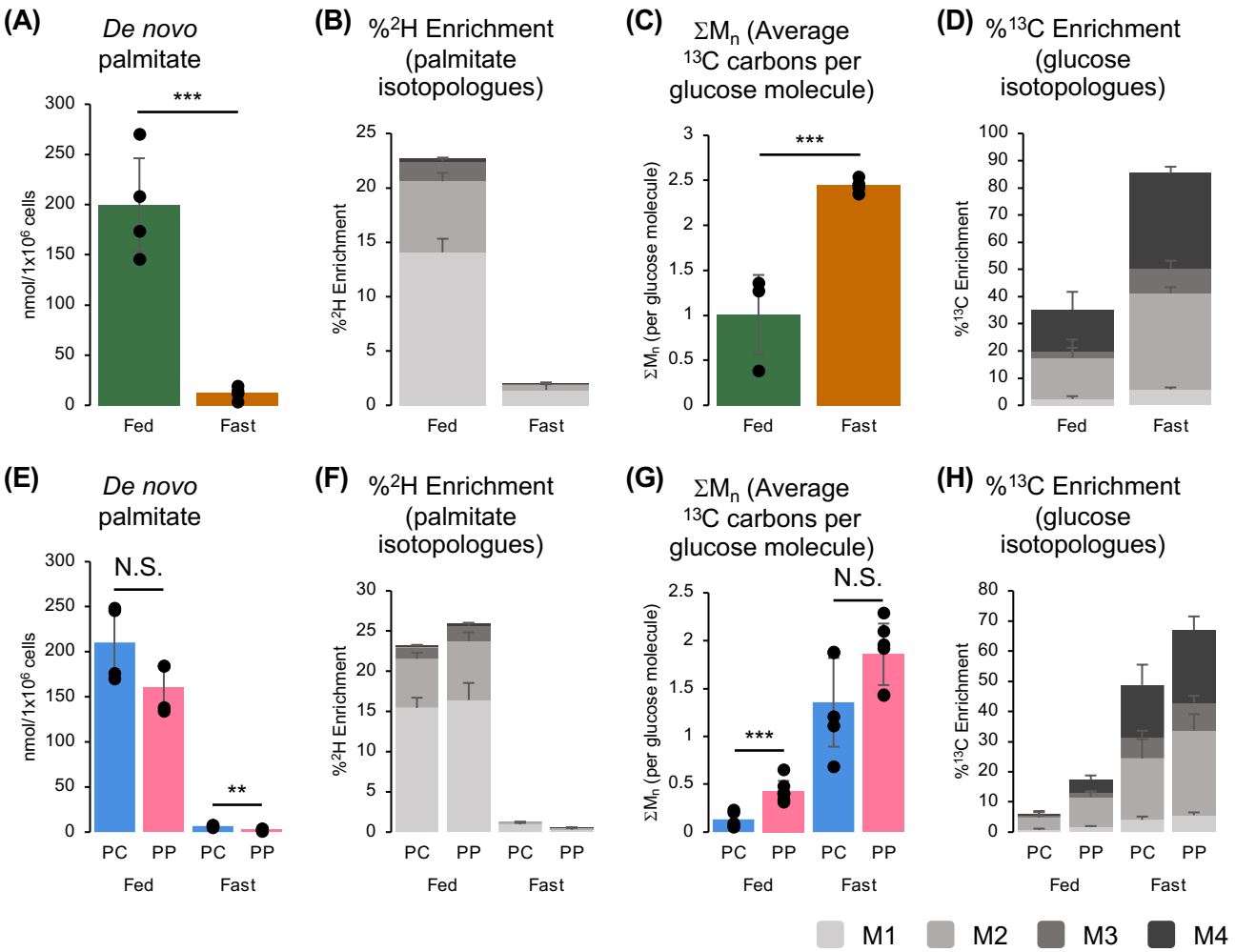

Figure 5 – A subset of liver regions has higher ATP turnover in the fed state

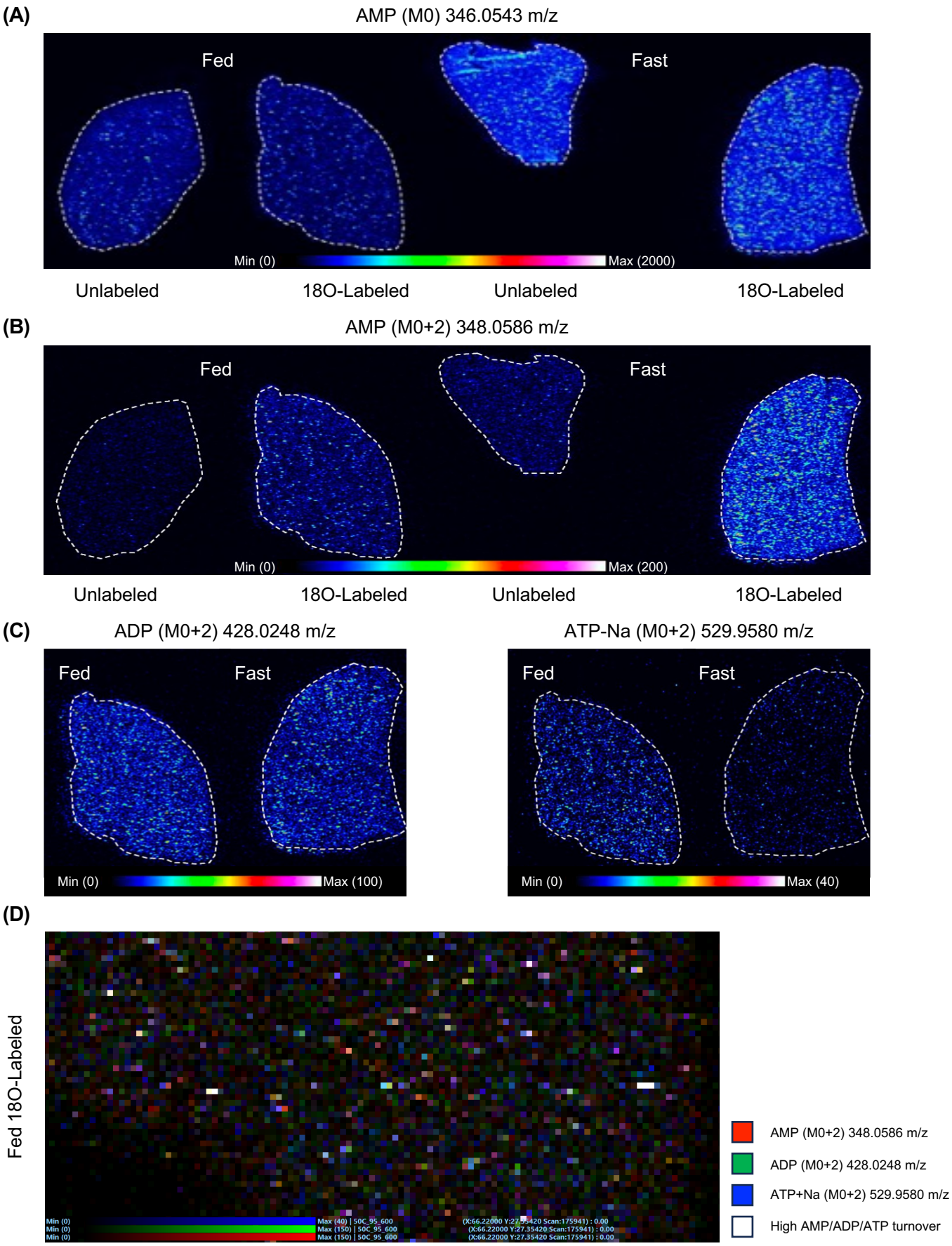

Figure 6 – A subset of hepatocytes is lipogenic and gluconeogenic

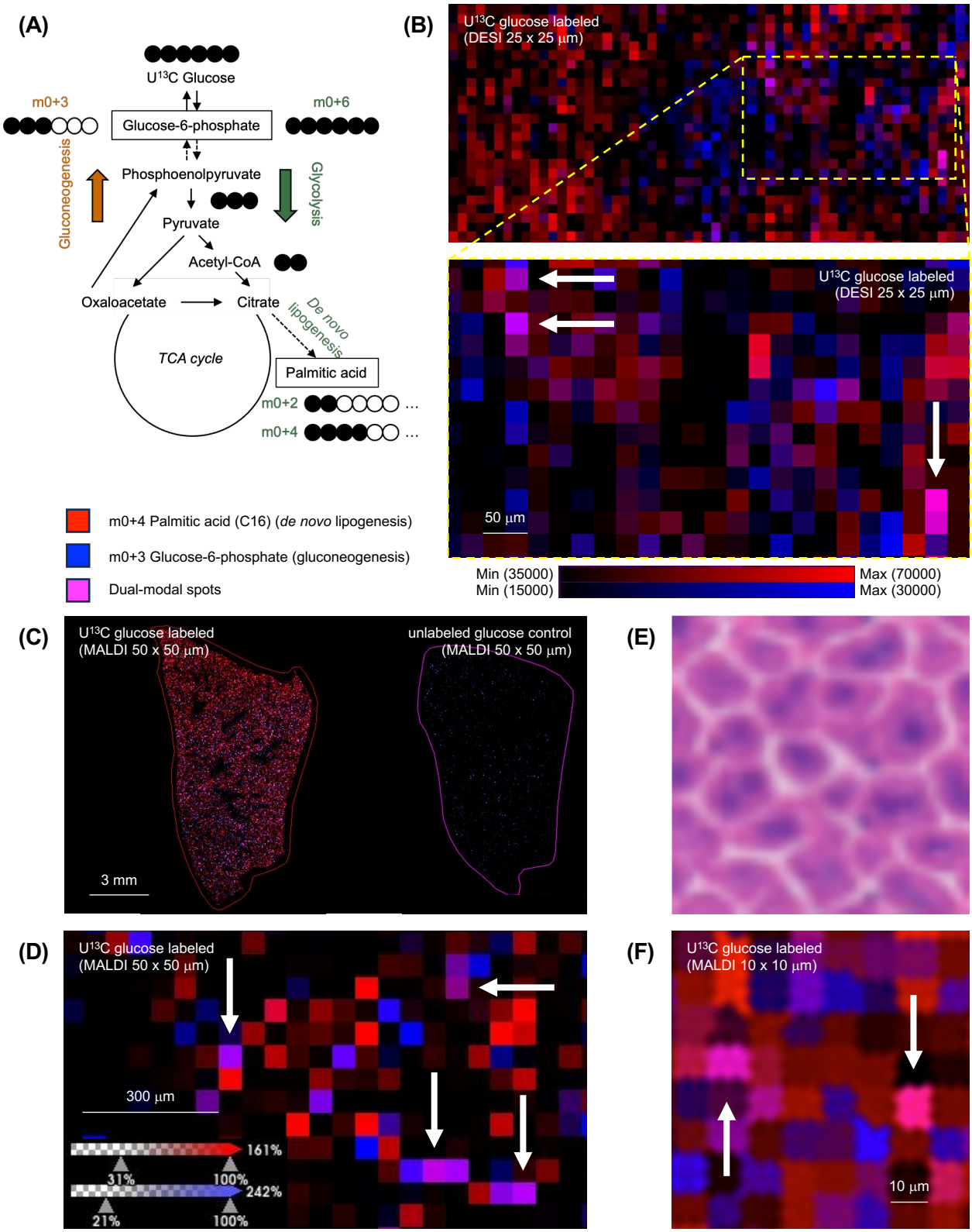

Figure 7 – Dual-positive spots increase in high-fat diet fed-mice liver

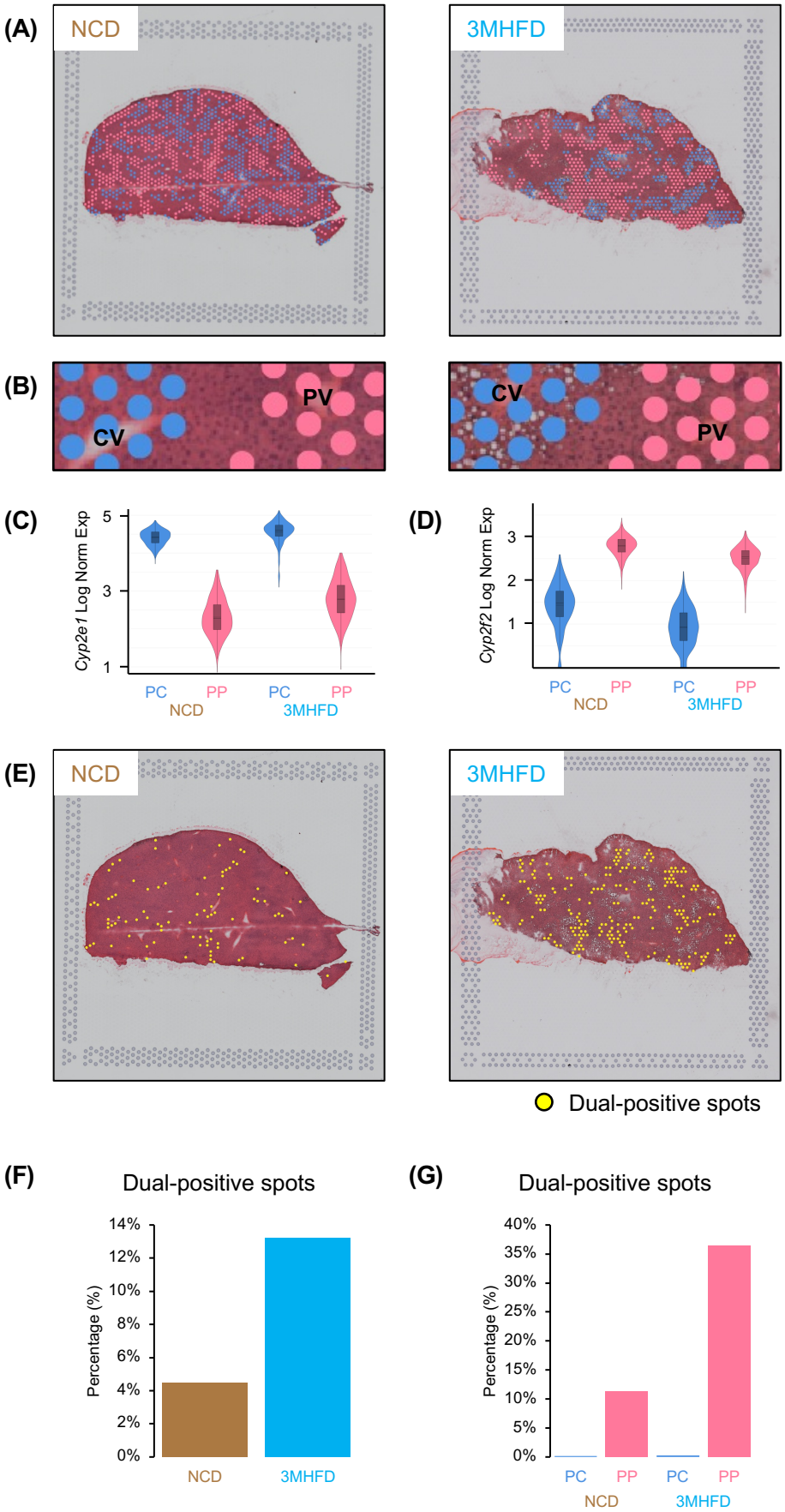

Supplementary Figures

Figure S1 – *G6pc* is transcribed in hepatocytes in the fed state

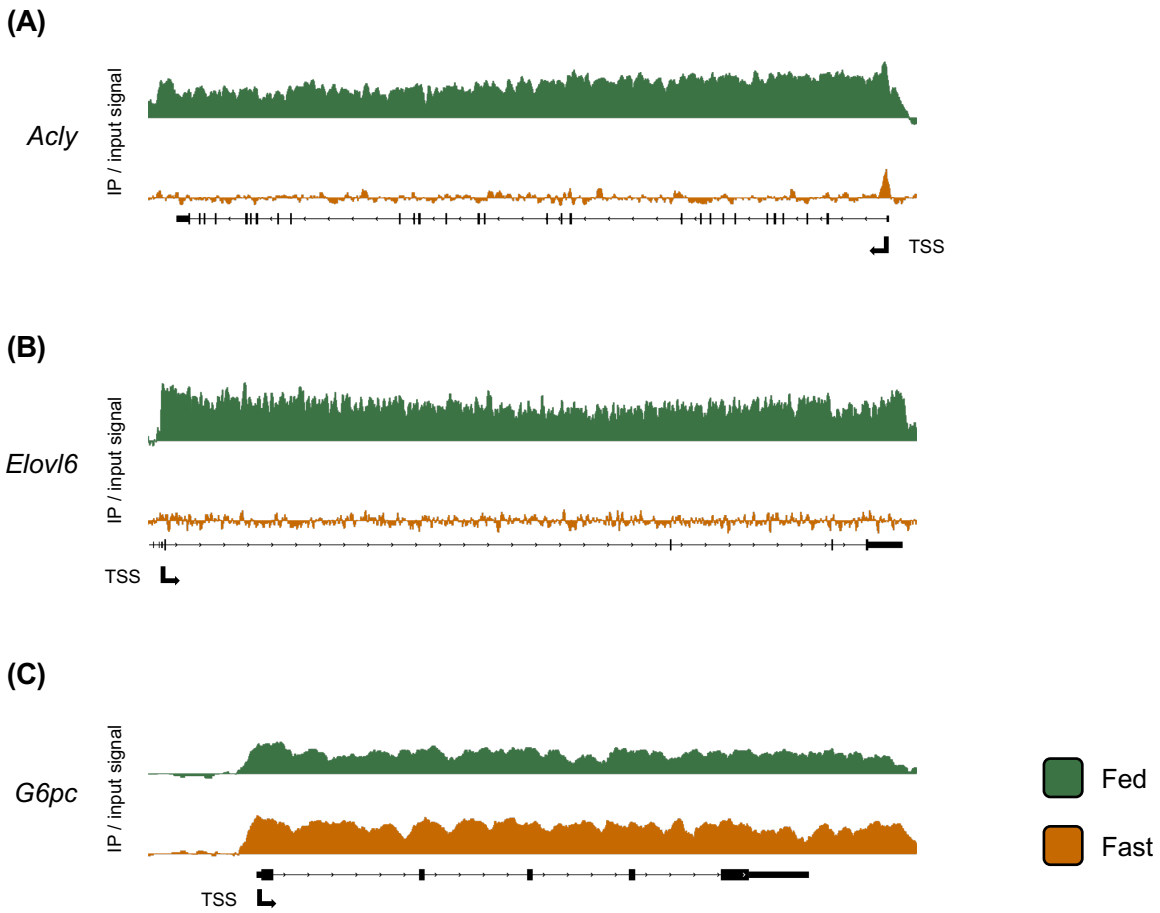

Figure S2 – *Pck1* is transcribed in periportal hepatocytes in the fed state

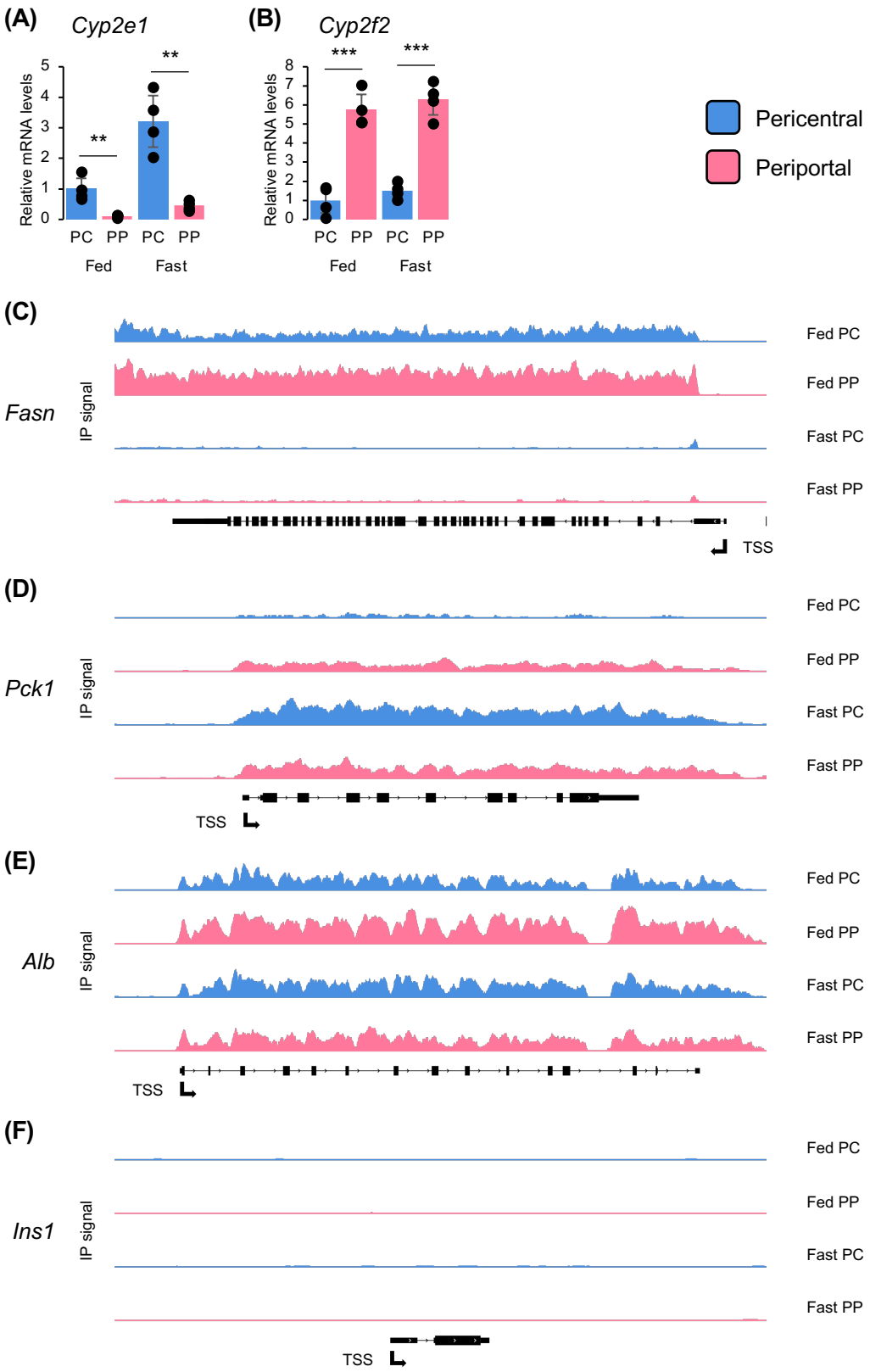

Figure S3 – Acly, Acaca, Elovl6, and G6pc are co-expressed in a subset of hepatocytes

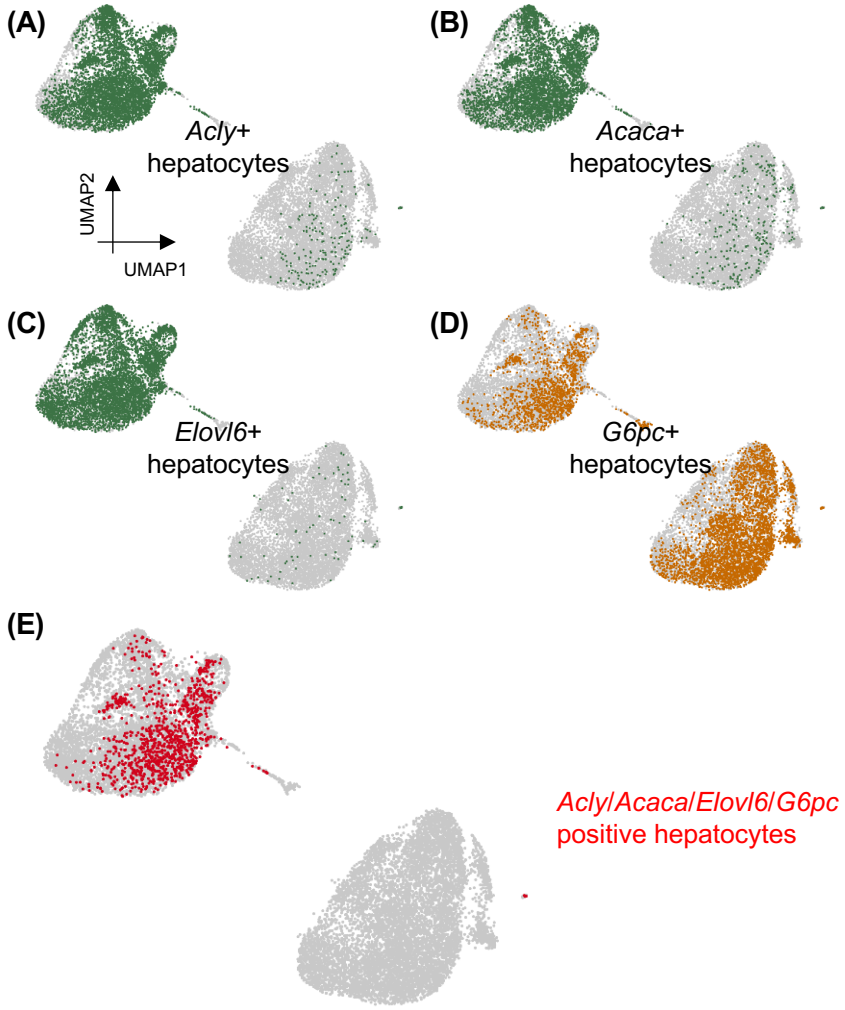

Figure S4 – *Pck1* is actively transcribed in the fed state

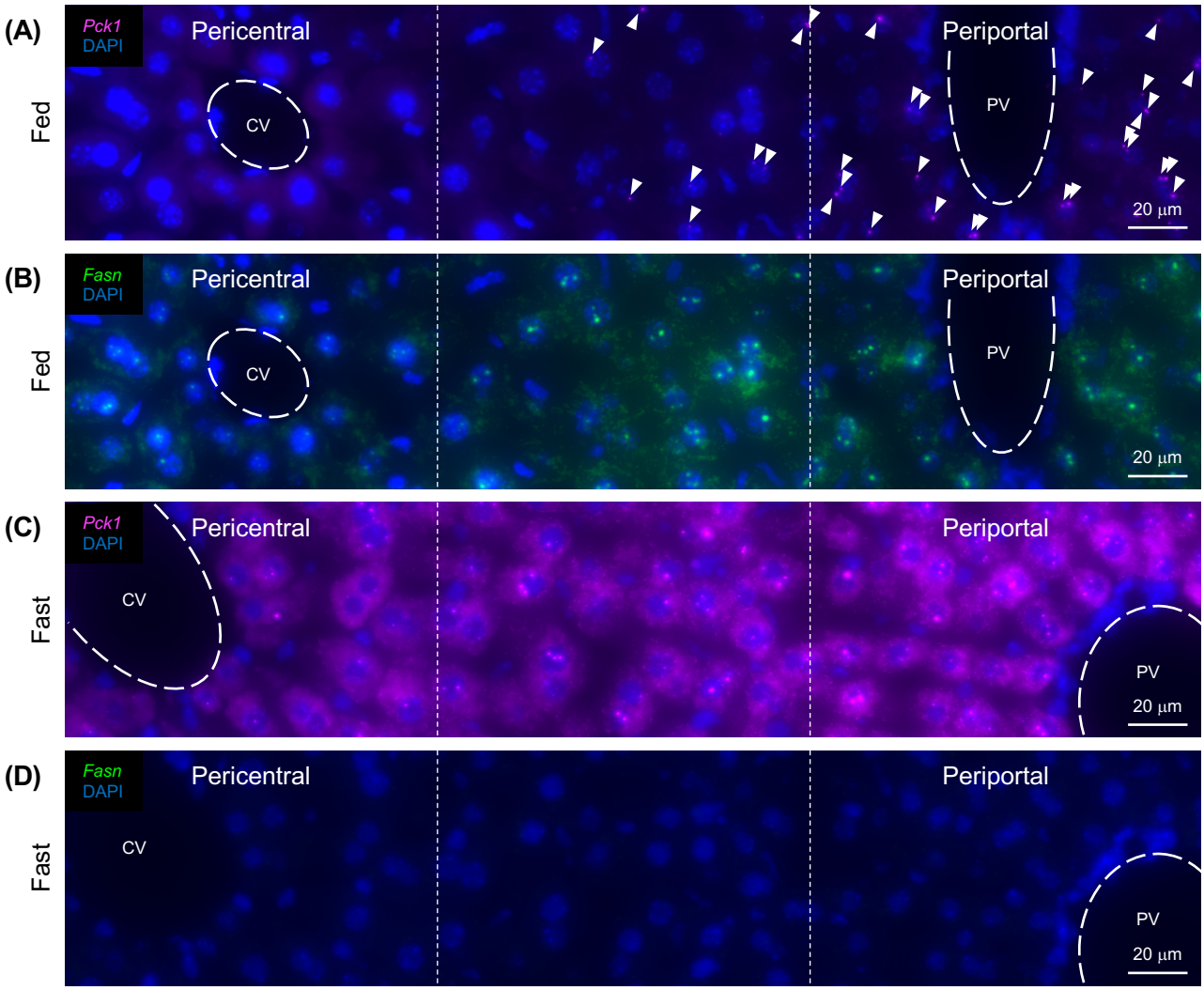

Figure S5 – Dual-positive hepatocytes are insulin resistant in suppression of *Pck1*

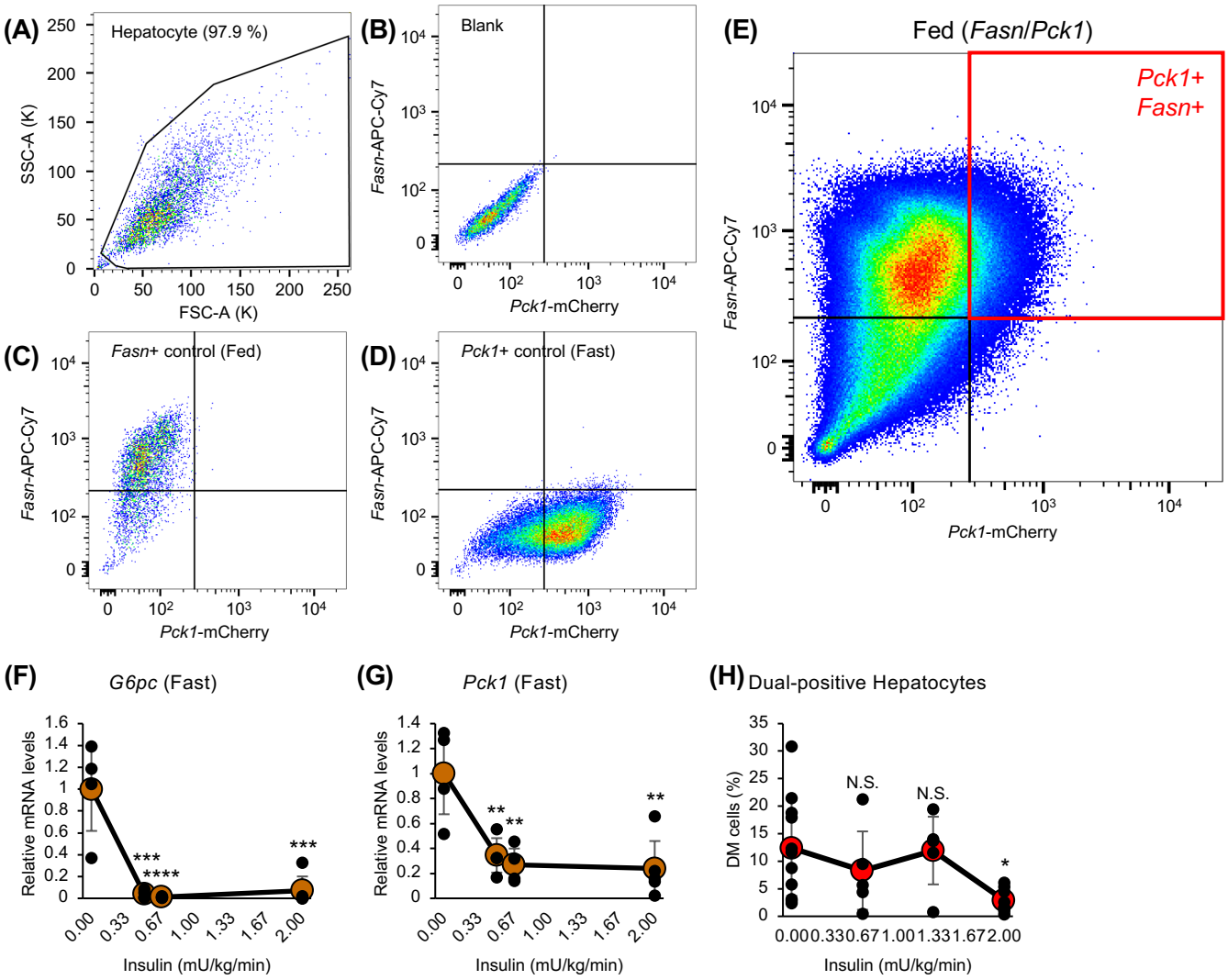

Figure S6 – Humanized mouse liver has dual-positive spots

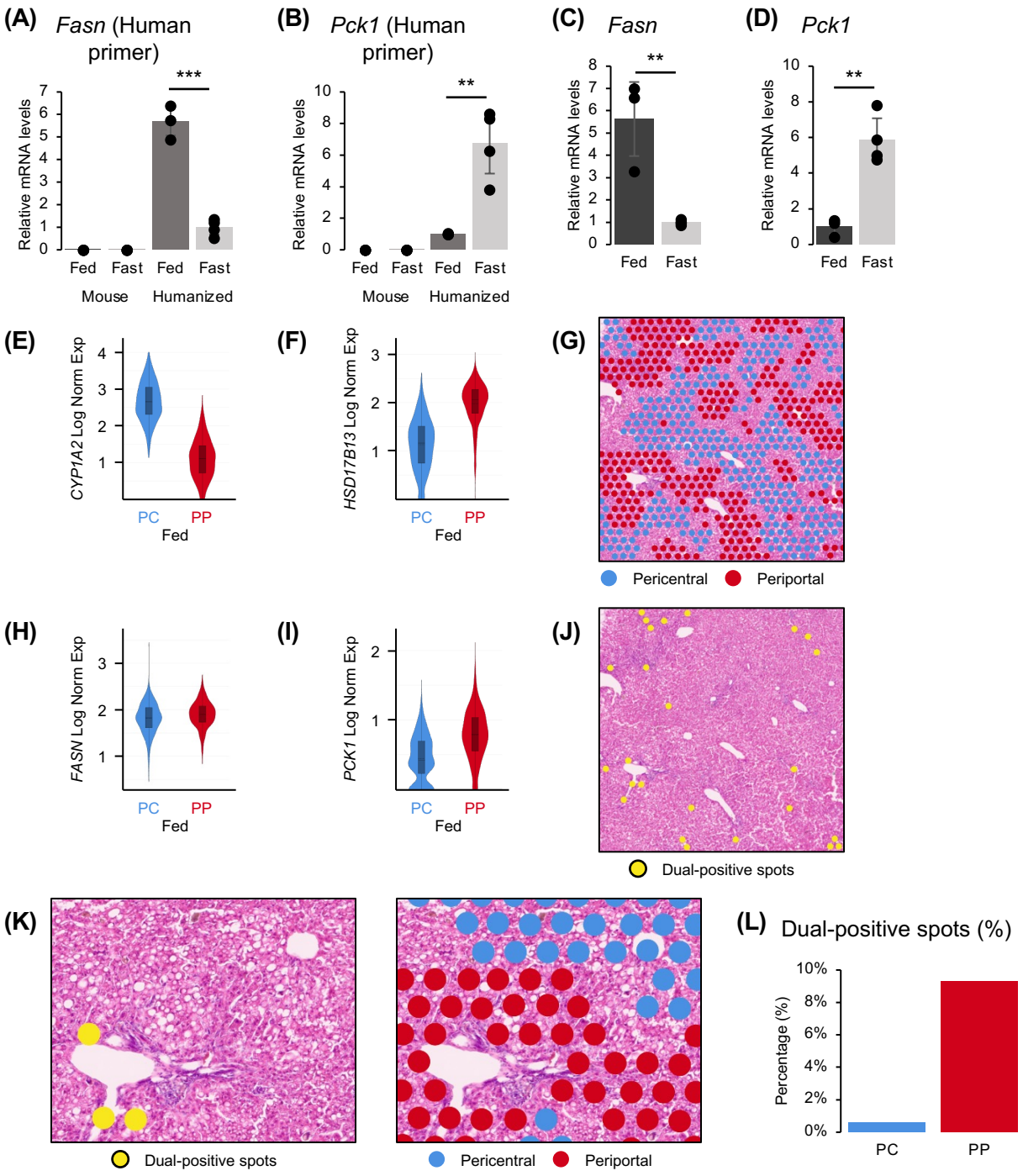

Figure S7 – t-SNE separates NCD and 3MHFD

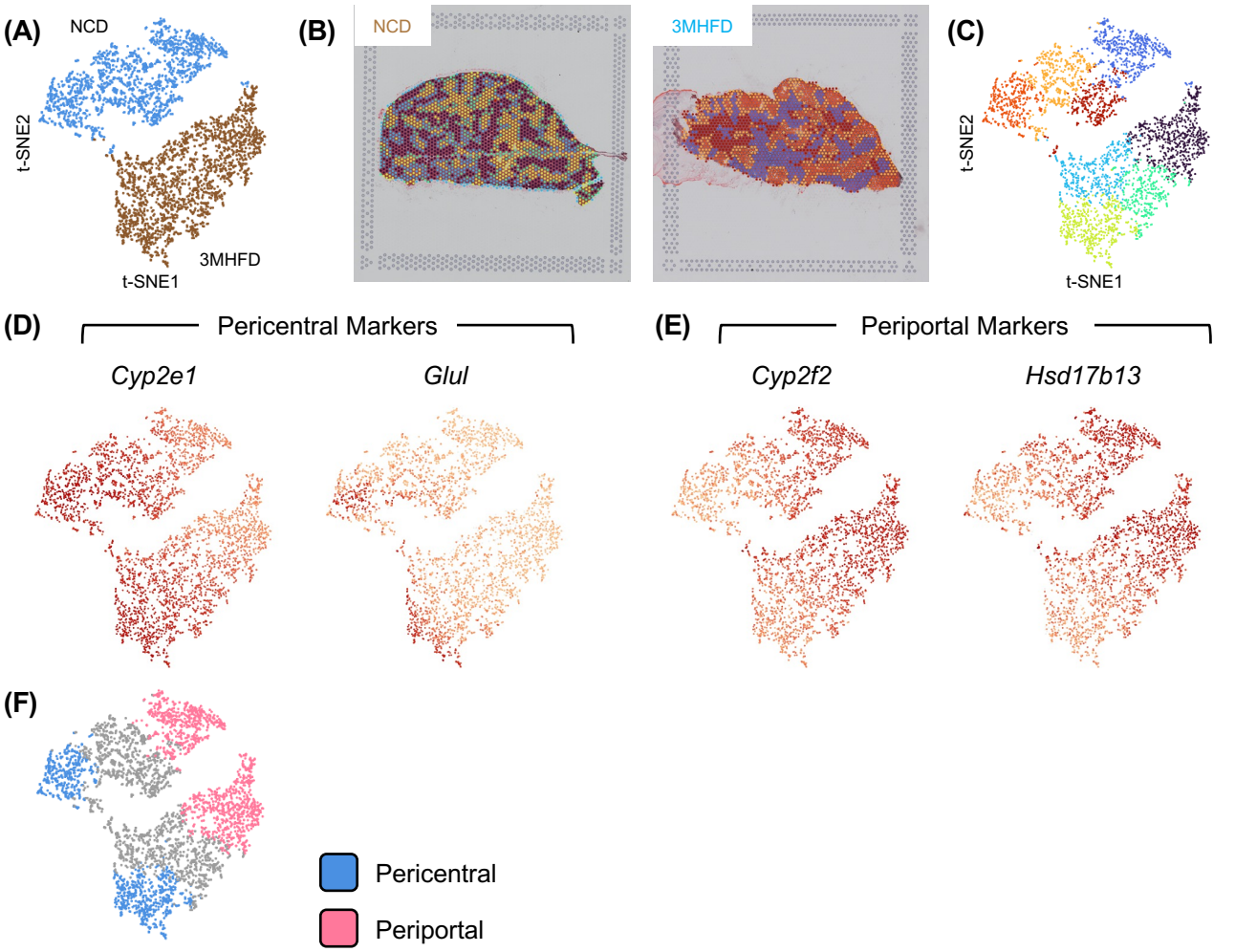

Table S1 – Compendium of $^{18}O/^{16}O$ exchange reactions which determine ATP turnover

Reaction:¤	Parameters:¤
γATP·+·[^{18}O]·H_2O·⟶·[^{18}O]·P_i·+·ADP¤	ATP·hydrolysis¤
[^{18}O]·P_i·+·ADP·⟶·[^{18}O]·γATP¤	ATP·synthesis¤
[^{18}O]·γATP·+·Cr·⟶·[^{18}O]·CrP·+·ADP¤	CK-catalyzed·phosphotransfer¤
[^{18}O]·γATP·+·AMP·⟶·[^{18}O]·βADP·+·ADP·⟶·[^{18}O]·βATP·+·AMP¤	AK-catalyzed·phosphotransfer¤

ATP turnover reflects the percentage of ^{16}O in ATP replaced by ^{18}O in the aliquot of cells analyzed, reflecting whole cell energetics. CK=creatine kinase, AK=adenylate kinase

Table S2 – Primer Sequences

Gene	Sequence (5' - 3')
Fasn _FWD (Mouse)	GGTCGTTTCTCCATTAAATTCTCAT
Fasn _REV (Mouse)	CTAGAAACTTTCCCAGAAATCTTCC
Pck1 _FWD (Mouse)	TCTCTGATCCAGACCTTCCAA
Pck1 _REV (Mouse)	GAAGTCCAGACCGTTATGCAG
Alb _FWD (Mouse)	CAAAGACGTGTGTTGCCGAT
Alb _REV (Mouse)	ACGGAGGTTTGGAATGGCAC
Cyp2e1 _FWD (Mouse)	CACAGCCAAGAACCCATGTACA
Cyp2e1 _REV (Mouse)	CAGGAGCCCATATCTCAGAGTTG
Cyp2f2 _FWD (Mouse)	CCTTTGACCCCGTGTTTATCC
Cyp2f2 _REV (Mouse)	TCGAAGCGACTTCCGAAGAC
Ppib _FWD (Mouse)	CAAGCATGTGGTTTTCGGCA
Ppib _REV (Mouse)	GCTGTCTGTCTTGGTGCTCT
Fasn _FWD (Human)	TTCTACGGCTCCACGCTCTTCC
Fasn _REV (Human)	GAAGAGTCTTCGTCAGCCAGGA
Pck1 _FWD (Human)	CATTGCCTGGATGAAGTTTGACG
Pck1 _REV (Human)	GGGTTGGTCTTCACTGAAGTCC
Ppib _FWD (Human)	AACGCAGGCAAAGACACCAACG
Ppib _REV (Human)	TCTGTCTTGGTGCTCTCCACCT